의학박사 학위논문

Metabotropic glutamate receptor 5 imaging and metabolic connectivity in pilocarpine-induced epilepsy rat model

필로카핀 유도 뇌전증 쥐 모델의 대사성글루타메이트 수용체5 영상 및 뇌 대사 연결성 분석

2014년 8월

서울대학교 융합과학기술대학원

분자의학 및 바이오제약학과

최 홍 윤

Contents

Abstract

Metabotropic glutamate receptor5 imaging and metabolic connectivityin pilocarpine-induced epilepsy rat model

Hongyoon Choi

Department of Molecular Medicine and Biopharmaceutical Science, Graduate School of Convergence Science and Technology, Seoul National University

Introduction

Epilepsy is a brain network disorder associated with dynamics of several neurotransmitters. Abnormal excitatory activities in epilepsy are mediated by neuronal changes ranged from molecular level to global connectomes.Metabotropic glutamate receptor 5 (mGluR5) that regulates glutamatergic neurotransmission contributes to epileptogenic network. Firstly, we investigated mGluR5 abnormalities in pilocarpine-induced epilepsy rat models using noninvasive *in vivo*PET imaging. As temporal lobe epilepsy (TLE) is associated with complex brain network, we investigated metabolic connectivity in the pilocarpine-induced epilepsy rat model and to evaluate feasibility of a new multi-scale network

framework applying to small-animal brain. We aimed to localize mGluR5 associated abnormalities and identified abnormalfunctional network in TLE. We also assessed a feasibility of a preclinical application of integrative imaging analyses to find molecular and global network changes in preclinical animals.

Methods

In vivo mGluR5 images were acquired using [^{11}C]ABP688microPET/CT in pilocarpine-induced chronic epilepsy rat models and controls. We also acquired microPET/CT atacute, subacuteas well as chronic periods after status epilepticus. Non-displaceable binding potential (BP_{ND}) of [^{11}C]ABP688 was calculated using simplified reference tissue model in a voxel-based manner. mGluR5 BP_{ND} of the rat brains of epilepsy models and controls were compared. We localized abnormal mGluR5 BP_{ND} in chronic epilepsy models using voxelwise analysis.

To find metabolic network abnormalities in chronic epilepsy rat models, [^{18}F]fluorodeoxyglucosePET was acquired in sixteen chronic models and ten controls to yield interregional metabolic correlation by inter-subject manner. Regional graph properties were calculated to characterize abnormal nodes in the epileptic brain network. Furthermore, a new multiscale framework, persistent brain network homology, was used to examine metabolic connectivity with a threshold-free approach and the difference between two networks was analyzed using single linkage distances (SLDs) of all pairwise nodes. To identify functional connectivity

of mGluR5 associated regions, we evaluated interregional metabolic correlation between the regions with significantly different mGluR5 BP_{ND}.

Results

Temporal patterns of mGluR5 BP_{ND} was found in [^{11}C]ABP688 PET study. In acute period after status epilepticus, mGluR5 BP_{ND} was reduced in the whole brain. BP_{ND} of caudate-putamen was restored in subacute period, while BP_{ND} of the rest of the brain was still lower. In chronic epilepsy rat model, BP_{ND} in hippocampus and amygdala was reduced on a voxel-based analysis. Using FDG PET images, we initially compared metabolic connectivity of chronic epilepsy rat model and controls. When interregional correlation of epilepsy rats and controls was compared directly, the epilepsy rats showed reduced connectivity involving left amygdala and left entorhinal cortex. Using graph theoretic analysis, the epilepsy rats showed reduced nodal and local efficiency in left amygdala. Persistent homology based network modeling showed a tendency of longer SLDs between left insula/left amygdala and bilateral cortical/subcortical structures in the epilepsy rats. The regions with significantly reduced mGluR5 BP_{ND} in epilepsy models showed reduced interregional correlation while those in controls showed strong correlations.

Conclusions

In vivo imaging of mGluR5 using [^{11}C]ABP688microPET/CT could find regional abnormal mGluR5 availability in dorsal hippocampus and amygdala of the pilocarpine-induced epilepsy rats. Epileptic brain in rats showed globally disrupted network properties on FDG PET based network analysis, particularly in the abnormal left limbic-paralimbic-neocortical network.Regional mGluR5 abnormalities were evidently accompanied by functional network disruption. The changes in mGluR5 availability and disrupted functional network suggest multifunctional molecular imaging in epilepsyprovide network abnormality in small animal brains as a preclinical research.

Keywords: epilepsy, mGluR5, [^{11}C]ABP688 PET, metabolic connectivity, graph theory, persistent homology

Student number: 2011-23073

List of Tables

List of Figures

Introduction

Epilepsy and metabotropic glutamate receptor 5

Epilepsy is a brain network disorder and associated with hyperexcitation of neurons. Because brain consists of complicate neuronal networks, ictal discharge initiates from cortical or subcortical structures and propagates to the other brain regions (1, 2). Excitation of neurons is mainly mediated by glutamatergicneurotransmission, which is important in the pathogenesis of epilepsy. In particular, metabotropic glutamate receptors (mGluRs) play a role in the initiation of epileptic discharge and propagation (3-5). Among them, group I mGluRs (mGluR1 and mGluR5) are associated with synaptic plasticity which underlielong-lasting depolarization and activate neurons to persistently hyperexcitable state in epilepsy(5-7). Therefore, there has been a growing interest in mGluR-mediated neuronal transformation and its global connections to develop spontaneous recurrent seizures and propagation, which contributes crucially to epileptogenesis.

The differences of mGluR expression in epilepsy were found *in vivo* studies as well as human specimen. In focal cortical dysplasia, strong immunoreactivity (IR) of group I mGluRs was observed in dysplastic neuronal cells suggesting a possible contribution to epileptogenesis(8). In human temporal lobe epilepsy (TLE), Blümcke, et al. reported up-regulation of mGluR1 IR was found though mGluR5 IR showed no significant change (9), however, Notenboom, et al. showed up-

regulation of mGluR5 in TLE patients, particularly in non-hippocampal sclerosis groups (10). In pilocarpine-induced temporal lobe epilepsy animal models, mGluR5 protein expression was decreased in hippocampus, the reduction of mGluR mediated hippocampal long term depression (LTD) was found (11, 12). Although there have been inconsistent results of group I mGluRs expression in epilepsy, the differences of mGluR are regarded as an important marker for epilepsy because of an evolving drug target (4, 13).

Metabotropic glutamate receptor 5 and neuronal modulation

mGluR5 is a G protein-coupled receptor. mGluR5 modulates various ion channels and intracellular messenger proteins, resulting in long-lasting modulation of neuronal excitability (14). The long-lasting modulation of neurons is a key feature in synaptic plasticity particularly in hippocampus. One of the changes is low-frequency stimulation related long-lasting synaptic depression, termed long-term depression (LTD), which is known to be related to mGluR5(15). The LTD involves many brain regions including the neocortex, hippocampus, striatum and cerebellum, which is regarded as a key molecular background of behavior, learning and memory (16). Furthermore, LTD has been considerably focused on a candidate for several brain disorders including Alzheimer's dementia (17), epilepsy (11, 18), autism and mental retardation (16).

Because of mGluR5 related synaptic plasticity and neuronal excitability,

mGluR5 has been recently regarded as an emerging drug target for brain disorders. In particular, symptoms of Fragile X syndrome, a genetic disorder characterized by mental retardation and autistic behavior, are alleviated by mGluR5 inhibitors (19-21). The downstream signals of mGluR5 are prevented by fragile X mental retardation protein (FMRP) and the process is associated with key pathogenesis of Fragile X syndrome (22). In terms of neurological hyperexcitability, mGluR5 inhibitors have been tried to other brain disorders including autistic disorders and epilepsy(22, 23). These trials ofmGluR5 related drugs come from previous success of Fragile X syndrome. Symptoms of Fragile X syndrome including autism and recurrent seizures are related to exaggerated response to mGluR5, which support the theory of mGluR5 related abnormal neuronal excitation (24, 25).

Metabotropic glutamate receptor 5 imaging

Recently, as a positron emission tomography (PET) tracer, 3-(6-methyl-pyridin-2-ylethynyl)-cyclohex-2-enone-O-^{11}C-methyl-oxime ([^{11}C]ABP688), has been developed using ahighly selective antagonist of mGluR5(26). ABP688 is based on the negative allosteric modulator, MPEP (1, 2-methyl-6-phenylethynyl-pyridine) (27). As one of the mGluR5 inhibitors, MPEP has been investigated for autistic disorders including Fragile X syndrome (28, 29). Therefore, taking a novel drug development for mGluR5 into consideration, mGluR5 imaging may provide pharmacodynamics as well as its anatomical distribution. Using [^{11}C]ABP688 PET,

in vivo molecular imaging of mGluR5 has been studied in various neurological and psychiatric conditions within humans as well as animals such as major depression or smokers (30, 31).

In order to measure receptor availability, several studies with regard to tracer kinetics were performed in humans and rodents (32, 33). Receptor densities can be measured by quantitative analysis of PET. PET imaging tracers such as [^{11}C]ABP688 are reversibly bound to the specific receptors, thus, they show binding reaction and eventually reach dynamic equilibrium. For tracer kinetics, to quantify the receptor density, binding potential (BP) is widely used. Specifically, binding potential is defined as the ratio of B_{max} (receptordensity) to K_D (radioligand equilibrium dissociationconstant)(34). K_D means inverse of binding affinity, thus, BP can be viewed as the product of binding affinity and receptor density. BP can be calculated by kinetic modeling and the measurement of concentration of specific regions.*In vivo* situation, plasma level of specific radioligand such as [^{11}C]ABP688 is varied according to its pharmacokinetics. For [^{11}C]ABP688 PET, the methods for quantification of receptor availiability are dependent on arterial blood samples as input function(32).For a rodent study, due to difficulties in arterial sampling, thereference tissue modelscan be alternative method. A reference region should show no specific binding of [^{11}C]ABP688 and similar with nondisplaceable binding as in the other brain region (35). Previous studies revealed that cerebellum was a suitable a reference region for [^{11}C]ABP688 binding. Reference region based PET

quantification was compatible with blood-sampling based methods for [^{11}C]ABP688(33).

As an evolving drug target and pathophysiologic role for several brain disorders, mGluR5 specific radioligands have been actively developed. Although [^{11}C]ABP688 is a specific and highly-selective tracer, relatively short half-life of ^{11}C limits its availability. Recently, overcoming its limitation, ^{18}F-labeled compounds have been developed, [^{18}F]FPEB(36). Furthermore, pathophysiologic importance emphasized, various radiolabeled tracers have been developed for metabotropic glutamate receptors, mGluR1 and 2 as well as mGluR5 (37). In the future, for clinical epilepsy imaging of mGluR5, those new compounds with good availability will be developed and their clinical usefulness will be clarified.

Epilepsy as a network disorder

In the view of epilepsy as a network disorder, regional changes in molecular level such as mGluR5 could not explain the entire complicated pathophysiology. In the clinical setting, patients with epilepsy generally undergo electroencephalography (EEG) and structural MRI to evaluate epileptogenic zone. However, the propagation of seizure activities from the seizure foci to the adjacent or remote areas is accompanied by various behavioral and cognitive symptoms. Nevertheless, we have been unable to explain language or other cognitive dysfunction with a confined epileptogenic zone localized by routine diagnostic

imaging studies (38, 39).

Functional neuroimaging studies such as [^{18}F]fluorodeoxyglucose (FDG) positron emission tomography (PET) or perfusion single photon emission computed tomography (SPECT) have been used to localize epileptogenic zones in epilepsy. Those imaging studies can provide brain metabolism or perfusion, which is closely related to neuronal activity (40-43).Recently, not only the localized functional abnormalities in the epileptic brain, but also the interregional connection abnormalities in brain network studies have been reported. EEG and functional or structural MRI studies as well as PET or SPECT were used to investigate network abnormalities (44-49). These approaches suggested that brain networks were disrupted in the epileptic brain, but the abnormalities were not confined to regional one in epilepsy patients.

Functional connectivity and network analysis

Functional connectivity is defined by statistical association or dependency between brain regions and it can be interpreted as neural interactivity(50, 51). Functional connectivity can be measured by fMRI, FDG PET, EEG, or MEG.An fMRI-based functional connectivity at rest, one of the most commonly used approaches, reflects neuronal correlates of spontaneous fluctuations inblood-oxygen-level-dependent (BOLD) signals between remote cortical regions(52). Quantitative metabolic measures using PET can be used for functional connectivity

because of coupling between neuronal activity and metabolism (53-55). While the fMRI-based functional connectivity measures temporal correlation of dynamic changes between brain regions, PET-based metabolic connectivity employedregional variations of metabolic demand in brain(56), with averaged minutes of temporal scale during resting state (i.e., interictal state in this study)(57-60). Since there is no validation study comparing PET-based connectivity to fMRI-based connectivity, and the two approachesmight provide different information due to differencesin energy consumption coupling(61, 62), along with fMRI-based functional connectivity and anatomical connectivity (e.g. diffusion tensor imaging), PET-based metabolic connectivity couldhave complementary rolein understanding brain functional connectivity.

To evaluate the complex brain connectivity, graph theoretic approaches were used to measure global topologic features and regional abnormal brain connectomes(63). Graph theory allows understanding the network characteristics of brain disorders as a complex system. Most of the graph theoretic analysis, including previous studies for the epileptic networks (46, 47), have used threshold to generate the binary networks because weighted network was difficult to interpret. However, when we construct brain connectomes, binary networks are varied according to the threshold, which results in the different graphs and network properties (64, 65). The problem regarding the threshold has been a challenge of network theory(66). Brain network is recently studied using the mathematical

graph theory, thus, there were few studies to solve network generation problem. A recently developed method provide threshold-free and multiscale network:Persistent brain network homology.The new multiscale framework of mathematicalmodeling for network was generated from all possible thresholds. Thus, it was free from the task of determining proper threshold (67).

Persistent homology based network analysis

Persistent homology can be used for topological data analysis which provides insight to the shape of data(68). Asimplicial complex is defined as a topological space constructed by vertex (0-simplex), edges (1-simplex), triangles (2-simplex), and their n-dimensional counterparts. A simplicial complex *K* by attaching simplices together should be satisfied the following conditions: any face of a simplex in *K* also belongs to *K* and the intersection of any two simplices in *K* is a face of each of two simplices. A dataset of points $\{x_i\}$can form a simplicial complex using the x_i as vertices, which can be visualized by adding higher orders. Rips complexis one of them whose k-simplices correspondto unordered (k+1)-tuples of points which are pairwise withindistanceε. Thus, Rips complex can be defined as a simplex formed by metric space and distance consisting of every finite set of points that has diameter at most ε. If a topologic data has a property that the distance between every pair of points in the set is at most ε, we include the topologic set as a simplex in the complex.

For brain network analyses, brain regions correspond to vertices and pairwise connections correspond to edges. To generate a binary network, threshold for distance allow us to visualize how brain regions are connected to each other. Because the complex would form differently according to the size of ε. Instead of deterministic ε to find topological features, the sequence of simplicial complexes as the distanceε increases, which is an approach of Rips filtration. Using this topological data analysis, networks generated by multiple thresholds can be summarized and visualized. A sequence of brain networks corresponds to Rips complex as we changed the threshold of distance, ε. The topologic parameter, Betti number β_0, is a measure of the number of the connected components in the network at the threshold of distance. We could visualize how the topological set of data is changed using barcode according to β_0. As ε increases, nodes are connected we visually identified how components are merged during Rips filtration, instead of attempting to determine an optimal threshold for brain networks generation.

Purpose

We investigated *in vivo* mGluR5 imaging in epilepsy rat model using [^{11}C]ABP688 PET to find temporal and spatial changes in the receptor density according to epileptogenesis. Furthermore, metabolic connectivity was analyzed using FDG PET in epilepsy rat models compared to controls.

In this study, we focused on *i)* regional abnormalities of mGluR5 as a candidate for epileptogenesis related marker, *ii)* large-scale functional network abnormalities measured by FDG PET, and *iii)* functional connectivity in abnormal mGluR5 associated networks in epilepsy rat models.

Though several brain disorders have revealed to underlie network abnormalities as well as molecular-level disruption particularly in neurotransmitter systems, there have been few studies focusing on linking the two approaches.Neurotransmitters affect specific neuronal synapses to change neuronal connectivity. For example, group I mGluR is closely associated with a network in the form of persistent activity states(69). As a microscopic level neuronal network, cellular imaging and electrophysiologicstudies showed mGluR5 activation enhanced neuronal connectivity. Furthermore,GABAergic activity asynchrony was closely influenced by mGluR1 and mGluR5 deactivation (70, 71). However, micro-scale level studies involving electrophysiologicand microscopic experiments have difficulties in investigating global brain dynamics. Because PET studies have advantages in noninvasively imaging molecular changes in global scale,evaluation of regional

molecular dynamics and construction of global brain networks are feasible. FDG PET can provide metabolic network driven by interregional variations of ‘minutes-scale’ glucose consumption in global brain. [^{11}C]ABP688 can show regional neurotransmitter status in global scale noninvasively.Thus, a combination of those two approaches could shed light on a mechanism of neurotransmitter driven network changes.

We studied temporal patterns of mGluR5 availability using [^{11}C]ABP688 PET after status epilepticus in a pilocarpine-induced epilepsy model.To investigate metabolic connectivity using FDG PET, brain networks were constructed for each group of rats by inter-subject manner. In the analysis of human brain images, several subject-specific factors (e.g. age and sex) should have been controlled but we could acquire homogenous group of epileptic brains in rat models. From those two experiments, we also proposed a new approach for combining molecular changes and global brain connectome. We expect to find localized molecular changes using noninvasive imaging study and abnormal metabolic connection in the brain of epilepsy rat models to explain various neuropsychiatric symptoms in medial TLE.

Methods

Establishment of epilepsy rat model

Adult male Sprague-Dawley (SD) rats (7 weeks old; Koatech, Seoul, Korea), weighing 180-200 g, were used for epilepsy rat models. They were kept at standard laboratory condition (22-24 °C, 12 hour light and dark cycle) with free access to water and standard feed. All the experimental procedures were approved by Institutional Animal Care and Use Committee at Seoul National University Hospital (IACUC Number 13-0224).

Rats were pretreated with lithium chloride (127 mg/kg, i.p., Sigma, St. Louis, MO) and methylscopolamine-bromide (1 mg/kg, i.p. Sigma) 24 hour and 30 min before pilocarpine administration, respectively. Pilocarpine hydrochloride (30 mg/kg, i.p., Sigma) was injected to trigger status epilepticus. Repeated doses of pilocarpine hydrochloride for 10 mg/kg were then administered every 30 min until stage 4 seizures developed according to the Racine scale (72). The control group received lithium chloride, methylscopolamine-bromide and saline (sham treatment) instead of pilocarpine. Status epilepticus was defined as continuous generalized seizures with stage 4 or 5 according to Racine scale without normal behavior between seizures. Diazepam (10 mg/kg, i.p. Samjin, Seoul, Korea) was injected 60 min after the onset of status epilepticus to terminate seizure activity.Repeated diazepam (5mg/kg) was administered unless status epilepticus was terminated to reduce mortality. After cessation of status epilepticus, rats were treated with

supplementary moistened and crushed pellets soaked in Gatorade® on the cage floor and given 5 mL i.p. injection of 0.9% saline for hydration in the rats unable to drink. The model rats in chronic period were monitored using a video recorder (12 h/day, for 2 days) to evaluate spontaneous recurrent seizure. Spontaneous recurrent seizures were observed in all chronic epilepsy rats which survived until PET studies.

Experiment 1: [^{11}C]ABP688 PET in pilocarpine induced epilepsy rat models

PET experiment design

To find temporal changes of mGluR5 availability after status epilepticus, PET scans were acquired at acute,subacuteand chronic periods in experimental group: acute period was defined as 1 day after status epilepticus, and subacute period defined as 7 days after status epilepticus. Because of general condition of rats, all the rats were not repetitively scanned for each period. Chronic period was more than 3 weeks after status epilepticus (median 44 d, range 34 d – 59 d). In 7 control rats, PET scans were acquired median 33 d (range 18 d- 52 d) after sham treatment. PET scans were successfully obtained for 4 rats in acute period, 4 rats in subacute period and 5 rats in chronic period after status epilepticus. [^{11}C]ABP688 PET experiments in this study were summarized in Figure 1.

Synthesis of [^{11}C]ABP688

ABP688 and desmethyl-ABP688 were prepared according to previously reported method (26) and all synthesized products were confirmed by ^{1}H-NMR and mass spectroscopy. All other chemical reagents were used as purchased without any purification.

[^{11}C]ABP688 synthesis was performed in a closed and lead-shielded hot cell by loop method(73). Briefly, 60% sodium hydride (5 mg, 0.12 mmol) was added to a solution of desmethyl-ABP688 (1 mg, 4.42 μmol) in anhydrous *N,N*-dimethylformamide (200 μL) and then the mixture was filtered. The resulting solution was loaded into stainless steel loop of injection port of HPLC. [^{11}C]CH_3I produced from [^{11}C]CO_2 using TRACERlab FX C Pro module (GE Medical Systems, Sweden) was passed through the loop and reacted with precursor at room temperature for 3 min. The product was purified by preparative HPLC(Xterra®preparative column RP8, 10 μm, 10×250 mm, Waters; mobile phase, EtOH:10mM NaH_2PO_4 [50:50], isocratic; flow rate, 4 mL/min). The purified [^{11}C]ABP688 (retention time of 10-11 min) was passed through a sterile Millex® FG and collected in a sterile vial. The final product was diluted with sterile saline for injection.

The radiochemical purity and specific activity of [^{11}C]ABP688 were determined by the analytical HPLC (Xterra® analytical column RP18, 3.5 μm, 4.6×100 mm, Waters; mobile phase, acetonitrile:water [50:50], isocratic; flow rate,

1.5 mL/min). The retention time of [^{11}C]ABP688 in analytical HPLC was 4-4.5 min.

[^{11}C]ABP688 PET acquisition

PET scans were performed on a dedicated microPET/CT scanner (eXplore VISTA, GE Healthcare). All animals were anesthetized and maintained with 2% isoflurane at 1-1.5 L/min oxygen flow and placed on the prone position under a scanner. Rats received an intravenous bolus injection (0.2-0.5 mL/rat) of [^{11}C]ABP688(7.0-17.1 MBq/100g) and list-mode data were acquired for 60 min with the energy window 400-700 keV. These list mode data were framed into a dynamicsequence of 6 x 30 s, 7 x 60 s, and 5 x 600 s frames.

All the images were reconstructed by a 3-dimensional ordered-subsets expectation maximum (OSEM) algorithm with attenuation, random and scatter correction(74). The voxel size was 0.3875 x 0.3875 x 0.775 mm.

[^{11}C]ABP688 PET preprocessing

Individual summed PET images were obtained from all rats (0-60 min summed images) followed by manual cropping of the necessary parts to include the entire brain. For seven control rats, images were spatially normalized to a representative brain. A voxel-based average brain image was constructed using nonlinear warping method after linear affine transformation. All transformations were performed

using BioImage Suite software package (www.bioimagesuite.org, Yale University) and registration was visually confirmed. In order to obtain [^{11}C]ABP688 PET template, the mean image was co-registered with a standard MRI T2 template using linear affine transformation(75). All the PET images including experimental and control groups were spatially normalized to the [^{11}C]ABP688 PET template (Figure 2).

[^{11}C]ABP688 PET kinetic modeling and parametric mapping

Regional time-activity curves (TACs) were calculated using the pre-defined volumes of interest (VOIs) defined on the rat template consisting of caudate-putamen, hippocampus, amygdala, frontal cortex, and cerebellum (75). For quantitative analysis, we used kinetic modeling analysis and generated parametric images of [^{11}C]ABP688 PET. Non-displaceable binding potential (BP_{ND}) was used to evaluate receptor availability, BP_{ND} was calculated by the simplified reference tissue model (SRTM) (35, 76) and the cerebellum was used as a reference region for the mGluR5 quantification(33).

Kinetic analyses and voxel-based BP_{ND} mapping were performed using MATLAB (MathWorks, Natick, MA) and C-based programs of Turku PET center (http://www.turkupetcentre.fi, Turku PET Centre, Finland). Parametric BP_{ND} maps were smoothened with a Gaussian filter of 1.2 mm full width at half maximum (FWHM). For voxel-based analysis, parametric BP_{ND} maps were used and the

VOIs were defined on the rat template.

Voxelwise analysis of mGluR5 BP_{ND} map

The BP_{ND} parametric maps of the rats in chronic period were compared with those of control rats on a voxel basis. Two-sample t-test was performed between two groups using statisticalarametric mapping software package (SPM2; University College London, London, England). Uncorrected values of $P < 0.001$ were set as the significance threshold and an extent threshold of 30 contiguous voxels was applied.

In order to evaluate the significance of changes in BP_{ND} of chronic epilepsy models, and to re-confirm the results of the voxel-based analysis, a post-hoc VOI analysis was performed using nonparametric Mann-Whitney test in clusters of the voxels with decreased BP_{ND}.

Immunohistochemistry

For immunohistochemical (IHC) analysisof mGluR5, rats (control, n = 2; acute period, n = 1; subacute period, n = 1; chronic period, n = 2) were sacrificed for staining of mGluR5 immediately after [^{11}C]ABP688 PET acquisition. Rats were anesthetized using tiletaminechloridrate-zolazepam (Zoletil) and perfused using 200 mL of phosphate buffer saline (PBS) for 10 min. The brains were removed and fixed in 4% paraformaldehyde (PFA) for more than 24 h and cut in 2 mm-thick

axial slices including hippocampus and caudate-putamen followed by paraffin embedding. 4 micrometer thick serial sections were prepared from these paraffin blocks. Endogenous peroxidasewas blocked in 3% H_2O_2 in PBS for 5 min. The primary antibody (mGluR5, 1:100 in antibody diluent; Novus Biologicals, Littleton, CO) was applied for 1 h. After washing in PBS, sections were incubated in biotinylated anti-goat secondary antibody for 30 min at room temperature, followed by avidin-biotin peroxidase complex for 20 min (Dako,Carpinteria, CA). Sections were colorized by peroxidase substrate diaminobenzidine (DAB) (Dako REAL^{TM} DAB and chromogen). Each section was photographed using a BX51 microscope (Olympus Optical Co, Japan). We assessed the IHC results as a visual confirmation study in the rats examined [^{11}C]ABP688 PET.The distribution and amount of immunoreactivity of mGluR5 receptor was qualitatively assessed by visual inspection, and compared with [^{11}C]ABP688 PET findings.

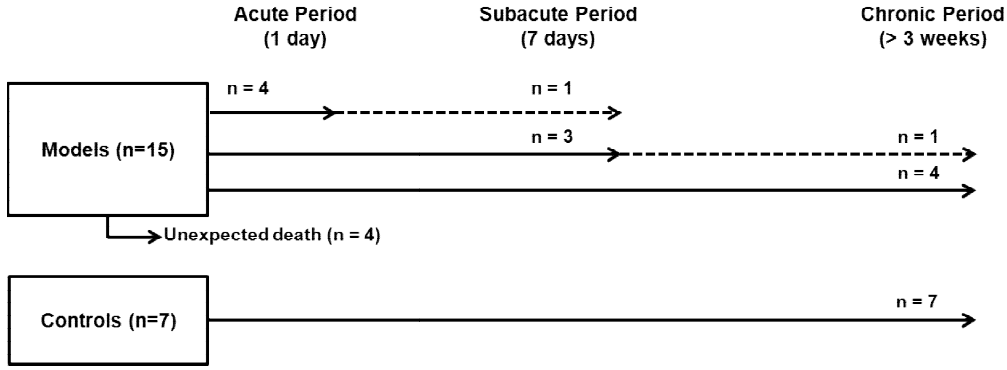

FIGURE 1.Study design for [^{11}C]ABP688 PET scans. After status epilepticus induced by pilocarpine administration, four rats were scanned in acute period. Three rats were scanned in subacute period without PET acquisition in acute period and four rats were scanned in chronic period after status epilepticus. Among the four rats scanned in acute period, a rat was scanned in subacute period and among the three rats scanned in subacute period, a rat was scanned in chronic period, repetitively (dotted line). (Choi H, et al. Plos One 2014)

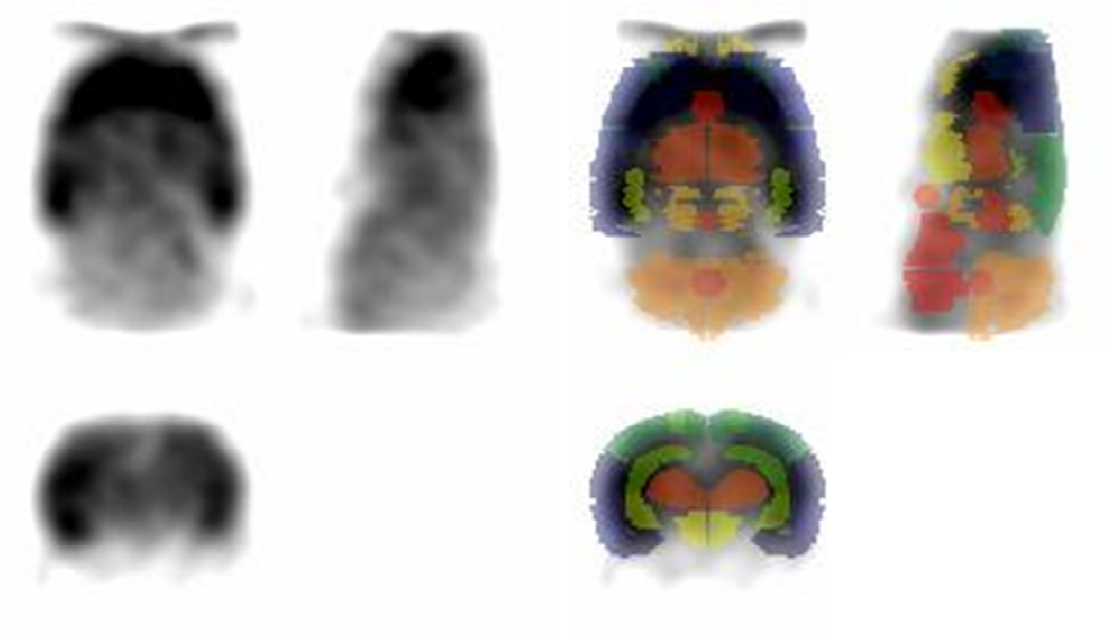

FIGURE 2.[^{11}C]ABP688 PET templates and predefined VOIs. To compare [^{11}C]ABP688 PET images from different groups, a brain template was generated. Coregistered summed images (0-60min) of all controls were transformed to a standard MRI T2 template and used as a PET template. All the PET images including experimental and control groups were spatially normalized to the [^{11}C]ABP688 PET template. Predefined VOIs were used to calculate regional receptor kinetics.

Experiment 2: Metabolic connectivity analysis

PET experiment design and FDG PET acquisition

FDG PET scans were acquired in chronic epilepsy rats and controls, which were different animals from [^{11}C]ABP688 PET experiments. FDG PET images were acquired at 5 weeks after status epilepticus (range 28-42 d) in the model group. In control rats, PET scans were acquired at5 weeks (range 28-35 d) also.

For FDG PET scans, rats were anesthesized for 5-10 min and received an intravenous bolus injection (0.3-0.5 mL/rat) of [^{18}F]FDG (37 MBq/rat). After the injection, each rat was awake for the 35 min period of FDG uptake. Static emission scans started at 45 min, which was optimal time for static FDG PET scan in rodents (77). Emission scan data were acquired for 20 min.

All the images were reconstructed by a 3-dimensional ordered-subsets expectation maximum (OSEM) algorithm with attenuation, random and scatter correction (74). The voxel size was 0.3875 x 0.3875 x 0.775 mm.

FDG PET preprocessing and parcellation for connectivity analysis

We used 26 FDG PET images for the connectivity analysis: 16 PET images from models and 10 images from controls. Individual PET images were spatially normalized to the FDG rat brain template(75)(PMOD 3.4, PMOD group, Zurich, Switzerland) using Statistical Parametric Mapping (SPM2, University College of London, London, UK). Before preprocessing, all voxels of PET images were scaled

by a factor of 10 in each dimension to fit approximately human brain size. All PET images were spatially normalized using nonlinear registration after linear affine transformation. Normalized images were smoothened by Gaussian filter of 12 mm full width at half maximum. The images were segmented into 36 anatomical volume-of-interests (VOIs) (Table 1 with abbreviation of each VOI). We used VOI templates predefined by PMOD software, which was constructed on 3D digital map based on Paxinos and Watson atlas (78). Among the VOIs, we chose cortical, subcortical structures and cerebellum. The value of FDG uptake was globally normalized to the individual gray matter count using SPM2.

Functional connectivity and brain network construction

The method for brain network construction and network analysis procedures are summarized in Figure2. To generate brain network, nodes were represented by the VOIs. We acquired intensity-normalized FDG uptake in the VOIs of each subject and correlation coefficients were obtained. Pearson's correlation coefficients (r) between each pair of the VOIs were calculated in an inter-subject manner and correlation matrix (36 x 36) was obtained for each group, epilepsy rats and controls. A weighted undirected network matrix was constructed for epilepsy rats and controls, where strength of each connection was simply defined as correlation coefficients. We also generated distance matrix, where the distance (c_X) between the nodes was defined as c_X=1-r.This approach has been previously

usedseveral times to define metric between two vectors as a topological view of brain network(79, 80).

Direct connectivitycomparison: epilepsy rats vs. controls

To find statistical differences of connectivity between the epilepsy rats and controls, we performed permutation test on all possible connections. Correlation matrix for models and controls were transformed to Z scores using Fisher transformation. Randomly reassigned labels (i.e. models or controls) were permuted 10,000 times for each of 36 VOIs and interregional correlation matrices were calculated, followed by Fisher transformation. We obtained Type I error by the comparison between the observed Z score for each connection and Z score from permuted data. To define statistically different connections, false-discovery-rate (FDR) was used to correct for multiple comparisons at a threshold of $q < 0.05$.

ssing
Parcellation
Correlation Matrix
Network
Subjects
Metabolic Activities of
Volume-of-Interests
Subjects
Direct Cor
Comparis
Graph The
Measures
Persistent
Network F
• Graph Filtra
• Dendrogra
• Single Link

FIGURE 3.Flowchart of metabolic connectivity analysis. Firstly, we processed FDG PET images to be spatially normalized. Metabolic activities of each node were obtained by predefined volume-of-interests and interregional correlation coefficient was calculated. All possible connected links in the epilepsy rats and controls were compared. We employed multiscale, threshold-free network modeling framework, persistent homology, to find abnormal metabolic connectivity.(Choi, H. et al. NeuroImage 2014.)

Table 1. Volume of interests and abbreviation

Region Name	Abbreviation
Motor Cortex	Mot
Medial Prefrontal Cortex	MedF
Orbitofrontal Cortex	OrbF
Insula	Ins
Parietal Association Cortex	ParA
Retrosplenial Cortex	RSpl
Somatosensory Cortex	SS
Cingulate Cortex	Cing
Auditory Cortex	Aud
Entorhinal Cortex	Ento
Hippocampus - AnteroDorsal	HpA
Hippocampus - Posterior	HpP
Amygdala	Amy
Visual Cortex	Vis
Nucleus Accumbes Core/Shell	Acb
Caudate-Putamen	CP
Thalamus	Tha
Cerebellum	CB

Graph theory analysis

Graph theoretic measurements were used to compare the networks. Each group, we measured the graph theory parameters using only positive links (81), where weighted undirected networks were obtained using correlation coefficient matrix. In this study, regional network properties including nodal efficiency (E_{nodal}) and local efficiency (E_{local}) were evaluated for each node(82, 83). E_{nodal} and E_{local} allow us to evaluate regional topologic properties without specific threshold.For N nodes and K edges in a graph (G), $E_{nodal}$for node i is measured as:

$$E_{nodal}(i) = \frac{1}{N-1} \sum_{i \neq j \in G} \frac{1}{L_{i,j}}$$

where$L_{i,j}$is the minimum path length between node i and j. By definition, $E_{nodal}$is an inverse of the harmonic mean of the minimum path length between a given node and other nodes in the network. Thus $E_{nodal}$is closely related to the shortest path length of each node.E_{local} represents the global efficiency (E_{global}) of subgraphs of the neighbors of a given node. E_{global} is the harmonic mean of the minimum path length between all possible pairs of nodes in the network. Because the given node is not an element of subgraphs when E_{local} is estimated, it can reflect the fault tolerance of the network, which means how each of subgraphs containing proper network information when the given node is eliminated.In short, E_{global} and E_{local} are measured as:

$$E_{gbbal}\ (G) = \frac{1}{N(N-1)} \sum_{i \neq j \in G} \frac{1}{L_{i,j}}$$

$$E_{local}\ (G_i) = \frac{1}{N_G(N_G-1)} \sum_{\mathrm{j,k}\in \mathrm{G}} \frac{1}{L_{j,k}}$$

whereN_G is the number of nodes in the subgraphG_i.

For global network properties, we employed E_{global} and the characteristic path length ($L_{network}$). $L_{network}$ is the average shortest path length for each node.

$$L_{network}\ (G) = \frac{1}{N} \sum_{i\in G} \frac{\sum_{i\neq j\in G} L_{i,j}}{\mathrm{N}-1}$$

To find statistical difference, we used permutation test for global network parameters including E_{global} and $L_{network}$ as well as for local network parameters, E_{nodal} and E_{local}. The observed regional and global network properties were compared with the network properties iteratively calculated from 10,000 times of randomly reassigned groups and we obtained p-value. To calculate graph theoretic measures, we used Brain Connectivity Toolbox (https://sites.google.com/site/bctnet/).

Multiscale network analysis based on persistent homology

We used multiscale and threshold-free network modeling based on persistent homology to compare the networks of models and controls effectively. Detailed procedures to quantify topological features based on persistent homology weredescribed in a previous study(67).In brief, we used networks generated at every possible threshold and to simplify the computation burden, graph filtration techniques were employed.

Firstly, we generated a sequence of networks as we changed the threshold of distance (ε). When ε increased, topological features of binary networks were changed. As a topological view of brain network, Rips complex was used to represent simplicial complexes. Rips complex is defined as a simplicial complex consisting of nodes and edges, whose *k*-simplices correspond to edges of a (*k+1*)-simplices which are links of two nodes within distance ε. Rips filtration reflects the multiscale networks, the sequence of the nested Rips complexes over different scales. One of the topological features, Betti number β_0, is a measure of the number of the connected components in the network. We could visualize those topological changes using barcode and dendrogram according to β_0. As ε increases, nodes are connected and using dendrograms, we visually identified how components are merged during Rips filtration.

Single linkage distance (SLD) between the nodes was calculated, which is usually used in hierarchical clustering. Given the network with distance c_X, we calculated SLD (d_X), which was defined as:

$$d_X(x_i, x_j) = min\,[max_{l=0,\ldots,k-1} c_X(w_l, w_{l+1}) | \, x_i = w_0, \ldots \, , w_k = x_j]$$

SLD can visualize information diffusion during the graph filtration as a view of a network. When information of nodes diffuse to other nodes over the network, the information is mixed and shared with the connected components according to their size increasing. Using SLD calculated from persistent network homology, we could obtain the distance between two specific nodes after network construction without

specific threshold.

SLD was employed to find different connections between the epilepsy rats and controls. We constructed single linkage matrices (SLM), SLDs between all pairs of nodes. SLMs were constructed with randomly reassigned labels (i.e. models or controls) being permuted 10,000 times. Type I errorswere calculated by the comparison between the observed SLD for each connection and SLD from permuted data. We used uncorrected $p < 0.05$ to find significantly different connections.

Metabolic connectivity of mGluR5 abnormal regions

To elucidate functional connectivity changes in abnormal regions with mGluR5 availability, we additionally analyzed metabolic connectivity between the clusters where mGluR5 BP_{ND} was significantly reduced on [^{11}C]ABP688 PET in epilepsy rats. More specifically, the abnormal clusters were extracted from voxelwise analysis using a threshold of uncorrected values of $P < 0.001$ and 30 contiguous voxels in comparison of epilepsy models and controls. Pearson's correlation coefficients of normalized FDG uptake between the clusters were calculated in an inter-subject manner for each group, epilepsy rats and controls. This approach is different from formal analyses using anatomically defined VOIs. To analyze large-scale functional network, one of the important issues is how nodes are selected. In this analysis, VOIs were extracted according to the mGluR5 availability rather than

anatomically defined structures.

To find statistically significant connections of mGluR5 associated regions, permutation tests were also performed. Because four mGluR5 associated clusters were included in this study, a number of possible connections were six. Therefore, we applied Bonferroni correction, *i.e.* $p < 0.05/6$ to find significantly different connections.

Results

Experiment 1: Regional mGluR5 abnormality in epilepsy model

Time-activity curve for [^{11}C]ABP688

Figure 4 shows representative time-activity curves (TACs) of controls and models in acute, subacute, and chronic periods. TACs were drawn for 1) caudate-putamen, 2) hippocampus, 3) frontal cortex, and 4) cerebellum. In all models and controls, high mGluR5 bindings were observed in caudate-putamen, hippocampus and lower bindings were seen in the cerebellum. Temporal changes of TACs in pilocarpine-induced epilepsy models revealed globally decreased activity in acute period compared to subacute and chronic periods after status epilepticus as well as controls.

Temporal changes of mGluR5 BP_{ND} in acute and subacute periods

mGluR5 BP_{ND} of caudate-putamen decreased in acute period (1.53 ± 0.26) compared to controls (2.13 ± 0.45) (U= 0, p< 0.01 for acute period vs. control). In the hippocampus, mGluR5 BP_{ND} of epilepsy models decreased in acute (1.11 ± 0.20) and subacute (1.20 ± 0.18) periods compared to controls (1.63 ± 0.18) (U = 0, p< 0.01 for acute period vs. control and for subacute period vs. control). Similarly to hippocampus, mGluR5 BP_{ND} in the amygdala was decreased in acute (0.94

±0.18) and subacute (0.82 ± 0.10) periods compared to controls (1.33 ± 0.15) (U = 1, p< 0.05 for acute period vs. control and U = 0, p< 0.01 for subacute period vs. control) (Figure 5).

Parametric images of mGluR5 BP_{ND} were generated using SRTM. As shown in Figure 4D, in acute period, BP_{ND} decreased globally in the whole brain, including the caudate-putamen and hippocampus. The BP_{ND} of caudate-putamen recovered in subacute period though it was still low in hippocampus and amygdala. In chronic period, regional mGluR5 BP_{ND} in the hippocampus and amygdala VOIs (not confined to significant voxels within these regions, in that 'significant' means the clusters 1 or 2 in Figure 6) recovered in comparison to that of subacute period.

mGluR5 BP_{ND} of chronic epilepsy models vs. controls

Using predefined VOIs, mGluR5 BP_{ND} of each brain region of chronic models was calculated and compared with that of controls. There was no significant difference in regional mGluR5 BP_{ND} between chronic epilepsy models and controls for the above four regions and amygdala on VOI analysis. BP_{ND} of caudate-putamen was 2.08 ± 0.18 and 2.13 ± 0.45, BP_{ND} of hippocampus was 1.63 ± 0.18 and 1.52 ± 0.43 and BP_{ND} of amygdala was 1.33 ±0.15 and 1.19 ± 0.37, for controls and chronic models, respectively.

Voxel-based analysis revealed the areas showing the significant difference in BP_{ND} between chronic epilepsy and controls. As is shown in Figure 6A, four

clusters mainly involving the part of bilateral dorsal hippocampus and amygdala showed lower mGluR5 BP_{ND} in chronic epilepsy models than controls. Increased regional BP_{ND} was not found in the model rats.

Post-hoc analysis was performed on two clusters mainly in the left dorsal hippocampus and left amygdala among the four clusters because of relatively higher T-scores and larger cluster size (Figure 5B). BP_{ND} of the cluster 1, a VOI on dorsal hippocampus, was significantly lower in the models in chronic period than that of controls ($U = 5$, $p = 0.048$), and there was a trend for decreased BP_{ND} in chronic modelin cluster 2, a VOI on amygdala ($U = 6$, $p = 0.06$).

Immunohistochemistry of mGluR5

IHC analysis wascorrelated with the PET imaging results. As shown in Figure 5, the distribution of mGluR5 in the rat brains was mostly consistent with the findings of [^{11}C]ABP688 PET studies. We assessed qualitatively brain sections with mGluR5 staining by visual inspection. Compared to controls, mGluR5 immunoreactivity of a model rat in acute period was reduced globally and restored partially in subacute period. mGluR5 expression in caudate-putamen decreased in acute period but recovered partially in subscute period and finally to normal level in chronic period. mGluR5immunoreactivity in the hippocampus in subacute period was also reduced (Figure 7K). However, there was no difference between mGluR5 immunoreactivity in the hippocampus in chronic period (Figure 7L) and

that of controls (Figure 7I). This was in contrast to the reduced BP_{ND} in the hippocampus and amygdala of model rats in chronic period found on a voxel-based analysis of [^{11}C]ABP688 PET.

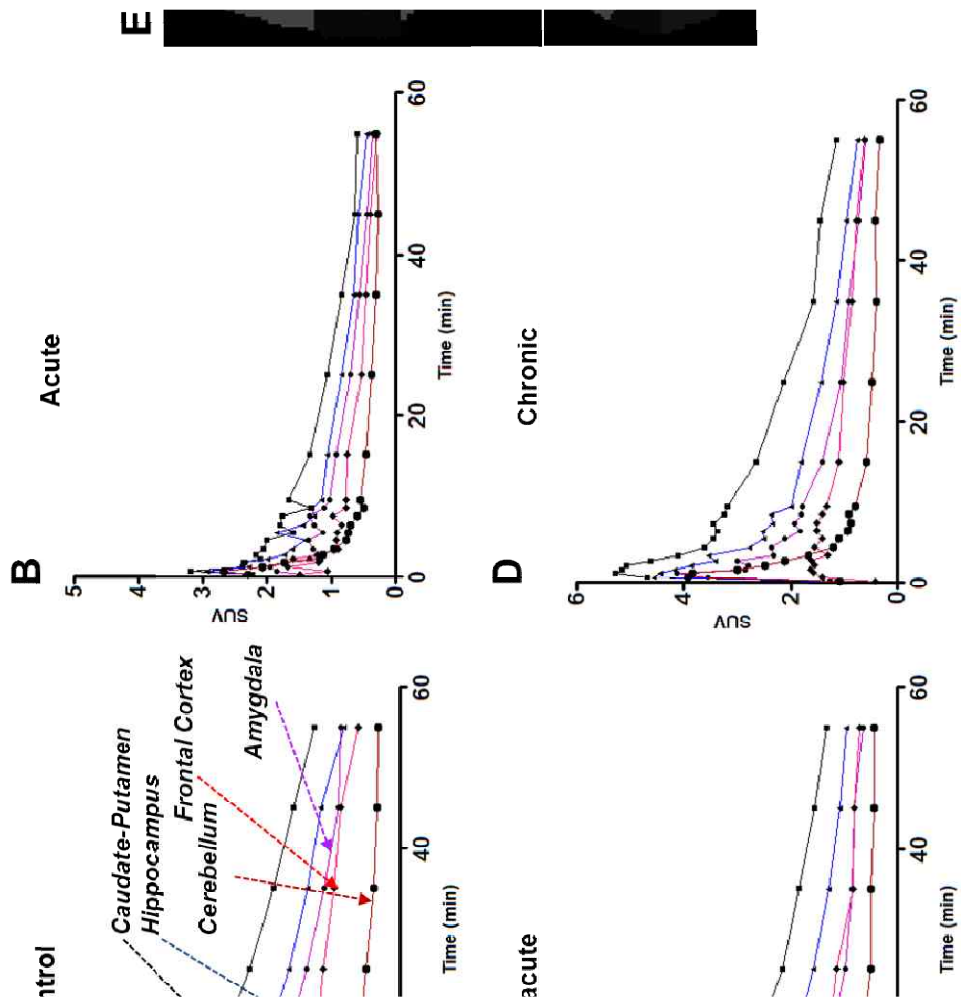

FIGURE 4.Representative time activity curves (TACs) of experimental epilepsy models. TACs in the caudate, hippocampus, frontal cortex, amygdala and cerebellum for 60 min with [^{11}C]ABP688 PET in the control (A), and epilepsy model rats in acute period (B), subacute period (C), and chronic period (D) after pilocarpine-induced status epilepticus. (E) Predefined VOIs for TACs and quantitative analyses. CP : Caudate-putamen; H: Hippocampus; F: Frontal cortex; Cb: Cerebellum, and A: Amygdala.

SUV: Standardized uptake unit, defined as activity (MBq/mL) within the volume of interest divided by the injected dose per body weight (MBq/g).

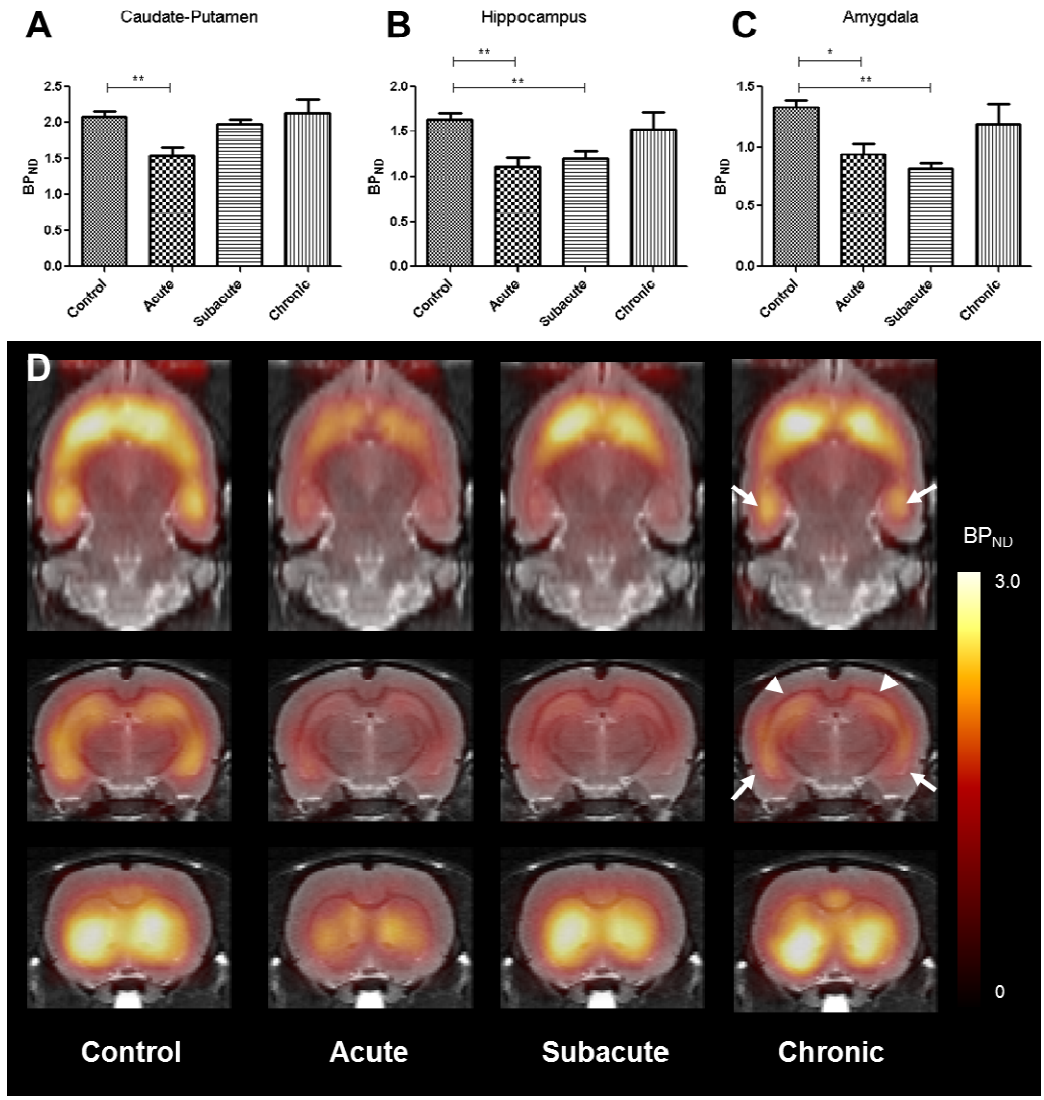
A
Caudate-Putamen
B
Hippocampus
C
Amygdala
BPND
Control
Acute
Subacute
Chronic
D
BPND
3.0
0
Control
Acute
Subacute
Chronic

FIGURE 5.mGluR5 binding potential (BP_{ND}) decreased in epilepsy models according to time periods after status epilepticus. (A-C) BP_{ND} decreased globally in acute period after status epilepticus. In subacute period, mGluR5 BP_{ND} recovered in caudate-putamen, while decreased yet in hippocampus and amygdala, and in chronic period, there was no significant difference in BP_{ND} between model rats and controls using VOI-based analysis. (D) Representative BP_{ND} parametric maps for model rats and controls were consistent with temporal patterns of VOI-based analysis. Note that $BP_{ND}$was visually normalized except in hippocampus and amygdala in chronic period, which corresponded to the voxel-based analysis (arrowheads: hippocampus, arrows: amygdala).

Error bars represent standard errors of the mean (SEM). * $p< 0.05$; ** $p < 0.01$.

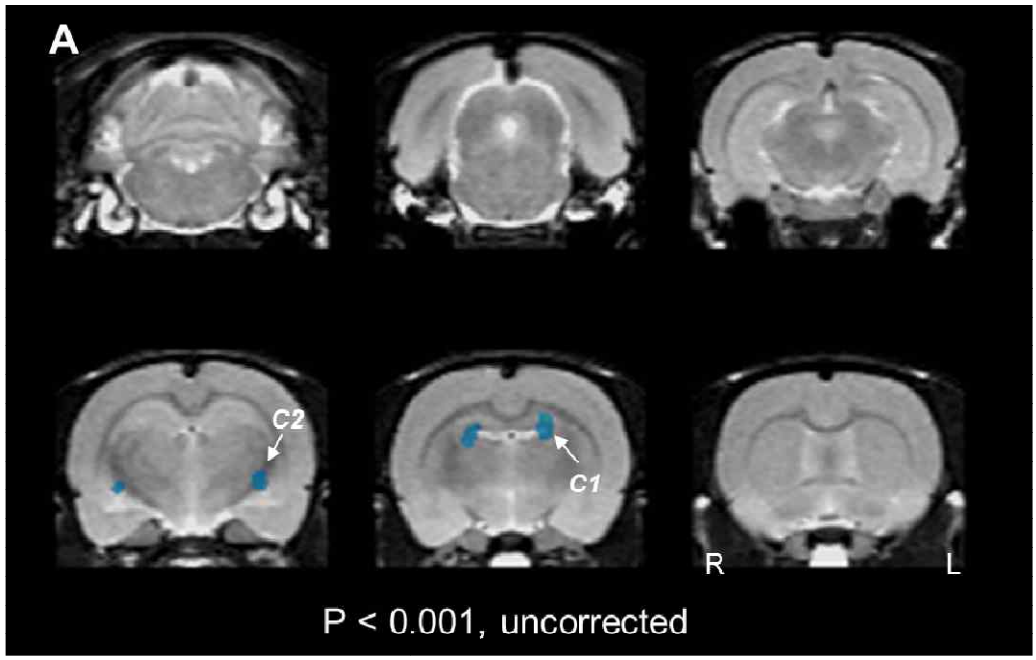
A
C2
C1
R
L
P < 0.001, uncorrected

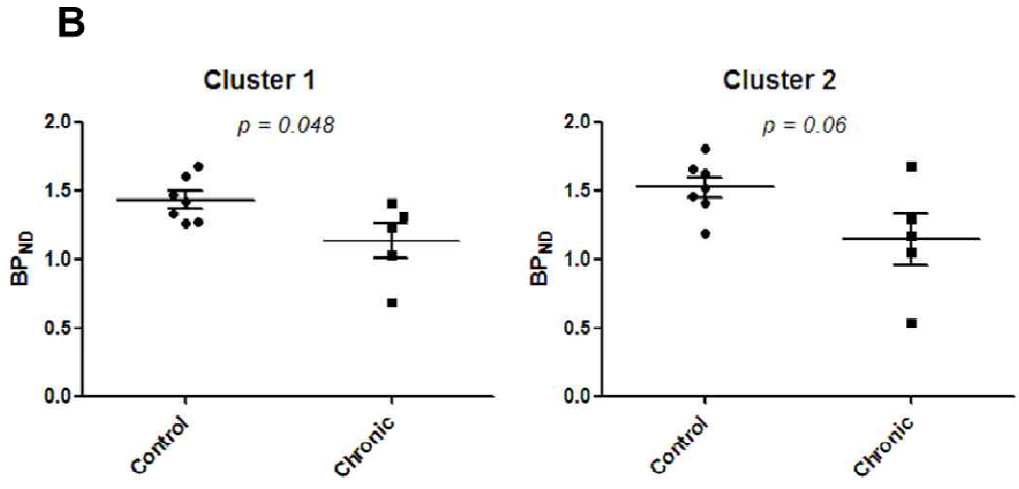
B
Cluster 1
p = 0.048
BPND
2.0
1.5
1.0
0.5
0.0
Control
Chronic
Cluster 2
p = 0.06
BPND
2.0
1.5
1.0
0.5
0.0
Control
Chronic

FIGURE 6.Spatial distribution of changes of mGluR5 BP_{ND} in chronic epilepsy model rats on [^{11}C]ABP688 PET. Compared with controls, BP_{ND} decreased in the bilateral amygdala and dorsal hippocampi (A: $p < 0.001$, uncorrected). (B) Nonparametric post-hoc VOI-based analysis performed on two clusters of decreased BP_{ND} on voxel-based analysis. BP_{ND} of cluster 1 (C1) on dorsal hippocampus in chronic epilepsy models decreased significantly compared to controls ($p = 0.048$). There was a trend for decrease in BP_{ND} of cluster 2 (C2) on amygdala in chronic epilepsy models compared to controls ($p = 0.06$).

B
C
D
F
G
H
J
K
L
CA3
CP
rol
Acute
Subacute

FIGURE 7.Regional distribution of mGluR5 using immunohistochemical analysis in sections of epilepsy models and controls.(A-D) Hippocampal sections were stained with H&E. In acute period, mGluR5 immunoreactivity of the epilepsy model rat decreased in caudate-putamen as well as hippocampus compared to controls (E-F) and recovered partially in subacute (G), and chronic periods (H). In the CA1 subregion, the intensity of mGluR5 staining decreased in acute, subacute periods compared to controls (I-K), and recovered in chronic period (L). DG : Dentate gyrus ; CP : Caudate-Putamen. Scale bars: 500 μm (A), 2 mm (E), and 100μm (I).

Experiment 2: Metabolic network abnormality in epilepsy model

Direct comparison of metabolic connectivity: Models versus Controls

We constructed correlation matrix for each group and Figure 8A and Figure 8B represent the c_X maps. For directly comparing the connectivity between controls and epilepsy models, permutation test was performed. Overall, the connectivity in the epilepsy rats was weaker than that in the controls (Figure8A-C). Epilepsy rats showed significantly longer c_X between the following pairwise VOIs: left amygdala-left somatosensory cortex, left amygdala-left caudate/putamen, left amygdala-both nucleus accumbens, left entorhinal cortex-left thalamus, left entorhinal cortex-right nucleus accumbens, and right posterior hippocampus-right nucleus accumbens ($q< 0.05$, FDR correction) (Figure 8D).

Characteristic regional and global graph theory measures in epilepsy rats

A trend toward globally lower E_{nodal} and E_{local}, local network parameters, was found in the epilepsy rats compared to the controls, which were observed in almost all the nodes. Among the differences of the nodes between epilepsy rats from controls, the difference in E_{nodal} and $E_{local}$of the left amygdala was the highest ($p = 0.017$ for E_{nodal} and $p = 0.007$ for E_{local}) (Figure9A and 9B). The differences of regional graph measures are shown according to their anatomical localization and summarized in Figure 9C and 9D.

Globally lower E_{nodal} and E_{local}in the epilepsy rats imply globally inefficient connections between nodes. These differences between epilepsy rats and controls were also found in the global network parameters, E_{global} and $L_{network}$. In the permutation tests, we found significantly lower E_{global} and higher $L_{network}$ in epilepsy rats than those in controls ($p = 0.038$ for $E_{global}$and $p = 0.047$ for $L_{network}$) (Figure10). These differences of the regional and global network properties were considered to represent the disruption of network integrities, thus, the network properties of epilepsy rats more random network topology than those of controls.

Persistent brain network homology revealed dysfunctional left limbic-paralimbic-neocortical network in epilepsy rats

As a threshold-free and multiscale network framework based on persistent homology provides evolutionary changes during the threshold increase, we compared brain networks of epilepsy rats and models in terms of how brain regions (nodes) are connected and clustered during graph filtration.

To visualize network changes during graph filtration upon multiscale brain networks, representative graphs were displayed at different filtration thresholds $\varepsilon = 0.05, 0.10, \ldots, 0.35$ in Figure 11. Clustering of the brain connections was slower in the epilepsy rats than controls while ε was increased. The SLD for the each group was computed and converted to the dendrogram displays in Figure 12. When ε increased, dendrogram (Figure12A and 12B) revealed that clustering occurred later

in the hippocampus, amygdala and entorhinal cortex, which belong to limbic and paralimbic system, than the other nodes in both the epilepsy and control groups. In epilepsy rats, the clustering was delayed more than in controls. For each connected component, models showed globally increased SLD compared to controls. This was shown again in single linkage matrix form (Figure12C and 12D).

Epilepsy rats showed a tendency of longer SLDs between some pairwise nodes which could be detected in the permutation tests. When multiple comparison correction (FDR < 0.05) was applied to find significantly different SLDs in the epilepsy rats from controls, there were no edges survived. When the uncorrected p < 0.05 was applied, to find the tendency of different connections in the epilepsy rats, multiple pairwise nodes (edges) showed longer SLDs, mainly involving the connections between left insular cortex/amygdala and bilateral cortical/subcortical structures (Figure13A and13B).

Metabolic connectivity of mGluR5 associated network

We extracted 4 significant clusters from mGluR5 BP_{ND} maps of chronic epilepsy models and controls: bilateral dorsal hippocampi and amygdala (Figure 6). To investigate whether those mGluR5 affected regions showed significant functional connectivity disruption, additional metabolic network analyses were performed. Figure 14showed normalized FDG uptake of each cluster in controls and the epilepsy models. We also obtained correlation coefficients between the

mGluR5 affected regions (Figure 15). Metabolic covariance patterns of models in the regions for subjects were different from those of the controls, the connectivity of mGluR5 associated clusters were disrupted. When the Bonferroni corrected $p < 0.05$ was applied, significantly reduced connections were found between the clusters, which included: left amygdala-left hippocampus, left amygdala-right hippocampus, right amygdala-left hippocampus, and right amygdala-right hippocampus.

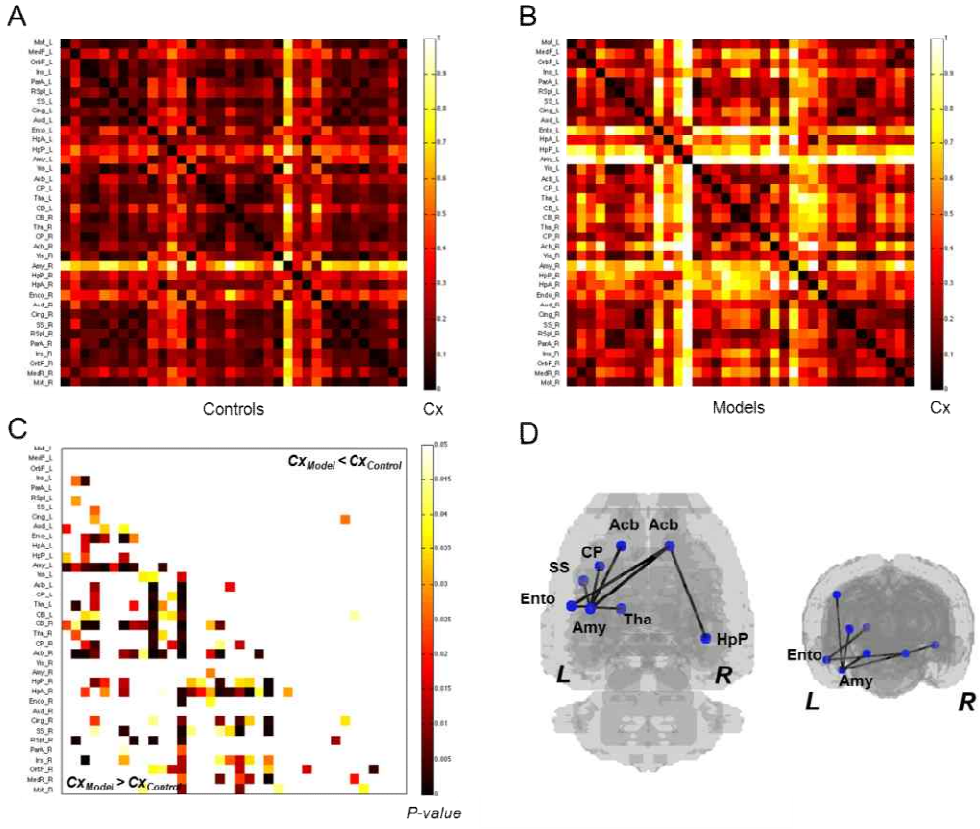
A
Controls
Cx
B
Models
Cx
C
$Cx_{Model} < Cx_{Control}$
$Cx_{Model} > Cx_{Control}$
P-value
D
Acb
Acb
CP
SS
Ento
Amy
Tha
HpP
L
R
Ento
Amy
L
R

FIGURE 8.Metabolic connectivity in the controls and epilepsy rats.(A-B) Distance maps for controls and epilepsy models, respectively. Distances (c_X) between two nodes (i, j) were determined by correlation coefficient (r), simply defined as $c_X(i, j)= 1-r(i, j)$. (C) To find statistically significant differences in metabolic connectivity between models and controls, we calculated p-values for all possible connections using permutation test. Statistical significance of increased metabolic connectivity (shorter distance) in the epilepsy rats is represented by upper trianglular matrix and decreased metabolic connectivity (longer distance) in the epilepsy rats is represented by lower trianglular matrix. (D) The anatomical distribution of significantly different links between epilepsy models and controls. In the epilepsy rats, significantly reduced connectivity was found in several pairwise nodes involving left amygdala and left entorhinal cortex ($q < 0.05$, FDR correction for multiple comparisons).

B
Control-Model
p = 0.017
Nodal
Efficiency
Control-Mo
p = 0.
Local
Efficienc
D
Nodal
Efficiency
Control-Model
Local
Efficie
Control
p-value
p-value

FIGURE 9.Difference in regional graph theoretic measures between epilepsy rats and controls. (A) Overall, nodal efficiency E_{nodal} in epilepsy rats was lower than that in controls. The largest difference was found in the left amygdala ($p = 0.017$, uncorrected for multiple comparison). (B) The epilepsy rats showed lower local efficiency E_{local} of each node, particularly in the left amygdala ($p = 0.007$, uncorrected for multiple comparison). (C-D) The nodes are displayed according to their anatomical location. The size of nodes represents difference between two groups and colors of nodes represent statistical significance.

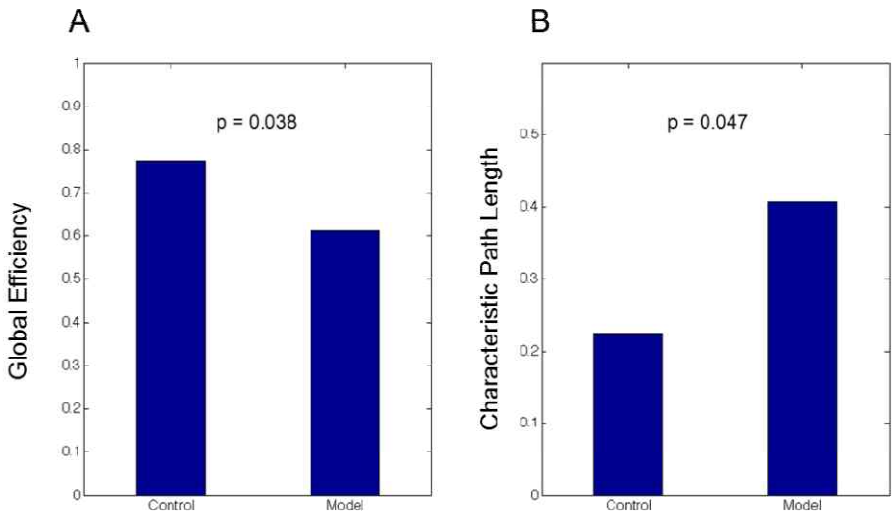

FIGURE 10.Global graph theoretic measures. The global network properties, global efficiency E_{global} (A) and characteristic path length $L_{network}$ (B), were displayed.Using permutation test, two parameters were significantly different between epilepsy rats and controls (p = 0.038 for global efficiency and p = 0.047 for characteristic path length).

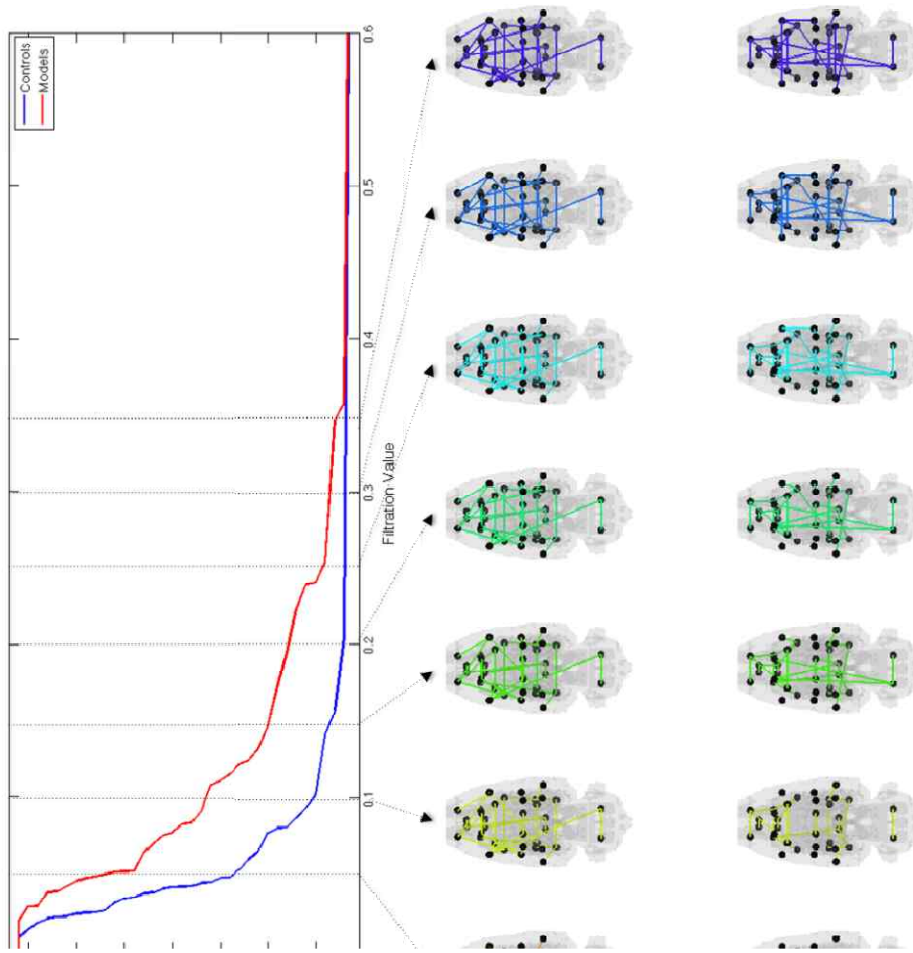
Controls
Models
Filtration Value
0.6
0.5
0.4
0.3
0.2
0.1

FIGURE 11. Graph filtration of epilepsy models and controls. The graphs are shown at seven different filtration values, $\varepsilon = 0.05, 0.10, \ldots, 0.35$. Note that nodes in epilepsy rats were clustered to giant single component with larger filtration values (distances) than in controls, suggesting globally disrupted and weak connections in epilepsy models.

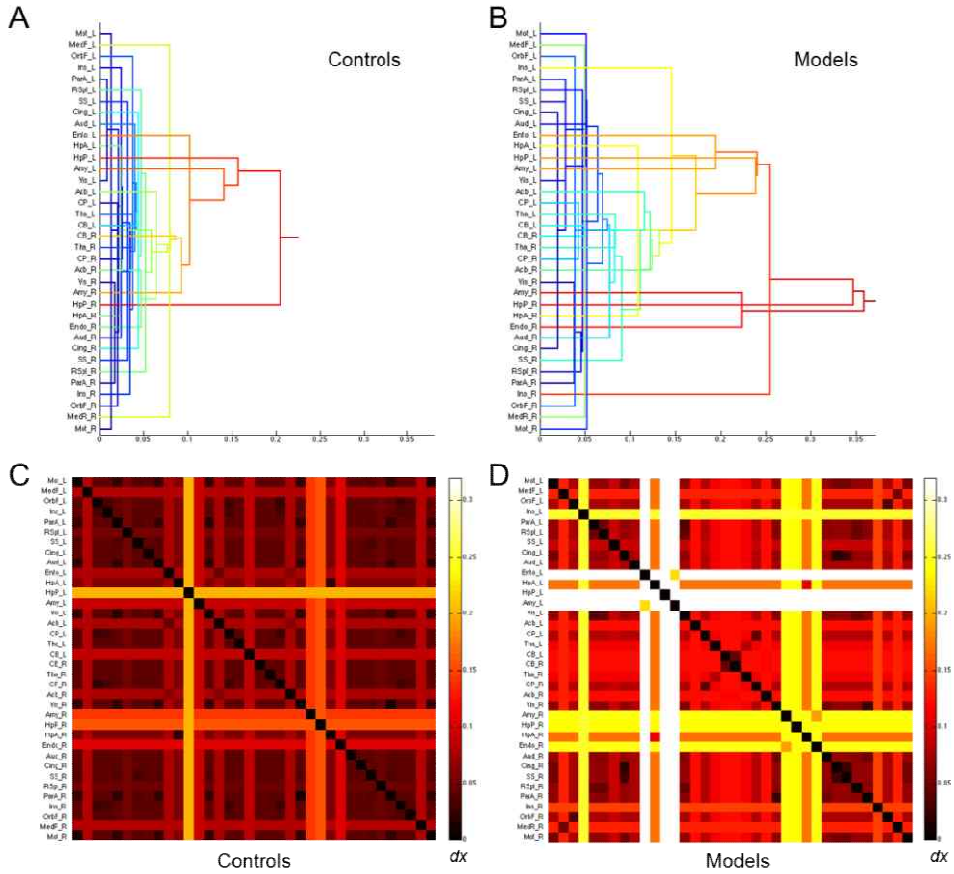
A
Controls
B
Models
C
Controls
dx
D
Models
dx

FIGURE 12.Single linkage dendrograms and single linkage matrices (SLM) for controls and models.(A-B) Dendrograms represent the evolutionary changes in linked nodes during graph filtration and distance to be merged into the giant component for each connected component. Limbic system showed delayed connections, particularly in the epilepsy rats. (C-D) SLMs calculated from the distance between the paired nodes in controls (C) and models (D). SLMs represented linkages from all possible thresholds and single linkage distances between all possible connections. Dendrograms show which components are merged during Rips filtration and SLMs reveal the recomputed distance between nodes according to the merging.

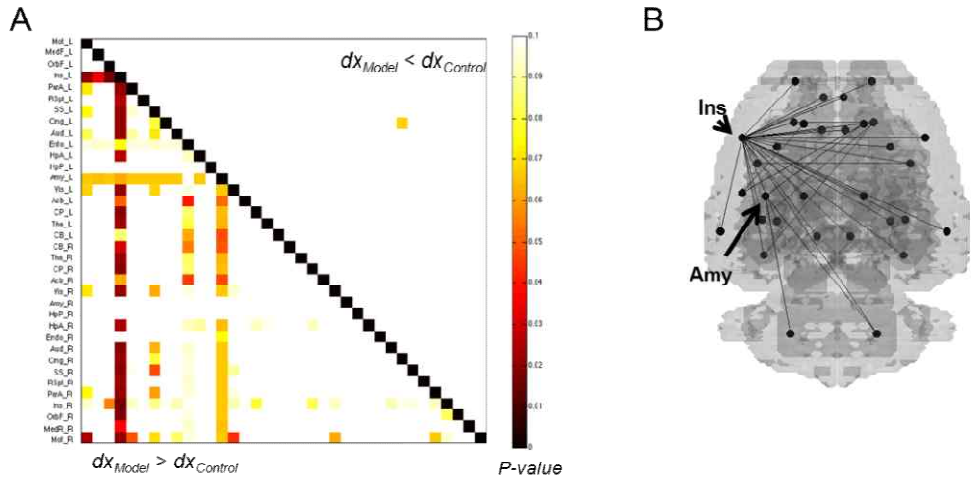

FIGURE 13.Group differences in single linkage matrices.(A) We calculated p-values for differences in single linkage distance between all connections using permutation test. Statistical significance of shorter distance in the epilepsy rats is represented by upper trianglular matrix and longer distance in the epilepsy rats is represented by lower trianglular matrix. (B) Using uncorrected $p < 0.05$ as a threshold, several connections with increased distance in the epilepsy rats were found. A tendency of increased single linkage distances in the epilepsy models was found in several connections, which mainly included left insular cortex and left amygdala.

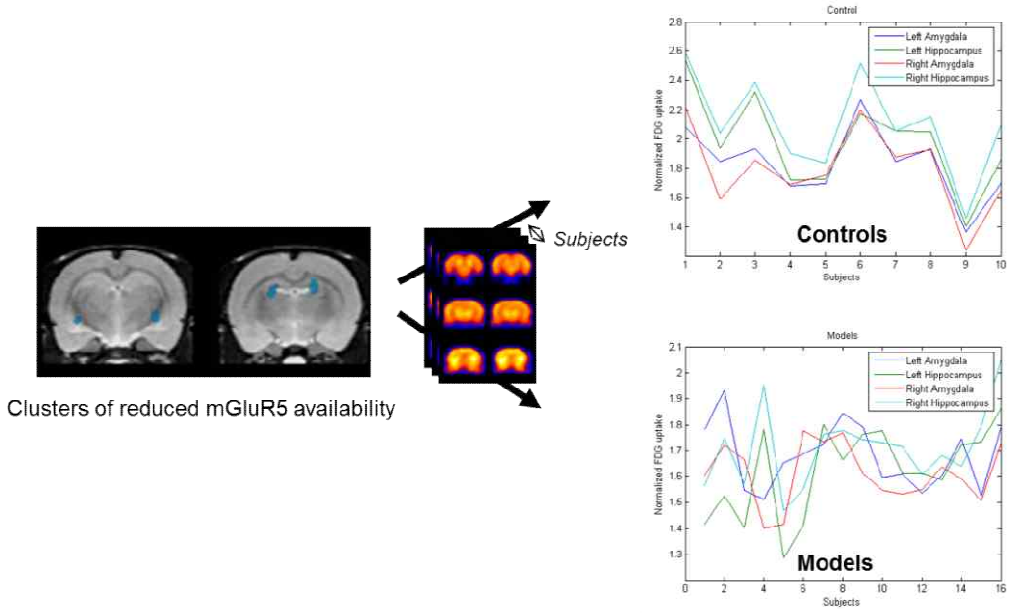

FIGURE 14. Metabolic covariance patternsin mGluR5 associated regions. Four clusters where mGluR5 BP_{ND} significantly decreased were used tofind metabolic covariance patterns. While controls showed synchronized FDG uptake (i.e. metabolic activity) between the clusters,epilepsy rat models showed discordant metabolic activity patterns across different subjects.

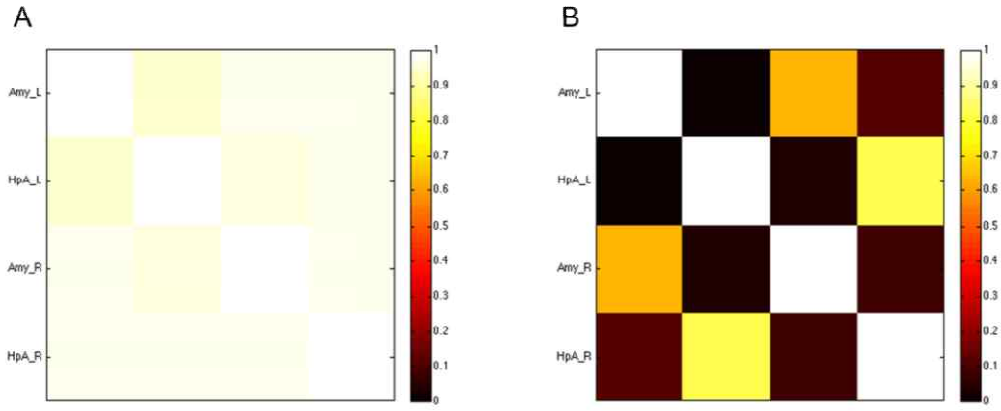

FIGURE 15. Metabolic connectivity in mGluR5 associated regions. Pearson correlation coefficients of the pairwise clusters where reduced mGluR5 BP_{ND} was found were more than 0.94 in controls (A). Compared to controls, correlation coefficients of the pairwise clusters were reduced in epilepsy (B). Significantly reduced connections in epilepsy rat models were included left amygdala-left hippocampus, left amygdala-right hippocampus, right amygdala-left hippocampus, and right amygdala-right hippocampus ($p < 0.05$, Bonferroni correction).

Discussion

We analyzed mGluR5 availability of the rat brain using [^{11}C]ABP688and metabolic connectivity in pilocarpine epilepsy rat models. From the first experiment of [^{11}C]ABP688 PET, a temporal pattern of mGluR5 BP_{ND} was found according to epileptogenesis. Using SRTM, we measured mGluR5 availability by BP_{ND}. We found a temporal pattern of mGluR5 BP_{ND} change after status epilepticus, that mGluR5 BP_{ND} decreased in the rat brain of epilepsy model globally in acute period after status epilepticus, restored but still decreased in hippocampus and amygdala in subacute period. In chronic epilepsy models, a voxel-basedanalysis and a posthoc comparison revealed that mGluR5 BP_{ND} in the dorsal hippocampus and amygdala was significantlylower than those of controls.

In metabolic connectivity analyses, direct comparison of the interregional correlation showed significantly decreased connectivity in the pairwise VOIs involving left amygdala and left entorhinal cortex in the epilepsy rats compared to controls. Graph theoretic measures were significantly different in the epilepsy rats compared with controls, which implied globally and regionally disrupted networks in epileptic brain. Furthermore, we used persistent homology based network analysis, which provided how networks were constructed and the linkages of nodes were clustered according to the changes of the thresholds. A tendency of weak connections was found between left insular cortex/amygdala and bilateral cortical/subcortical structures in the epilepsy rats.For connecting regional

molecular changes and functional connectivity, we measured metabolic connectivity between abnormal mGluR5 clusters, which also revealed severely disrupted connectivity in the epilepsy models.

mGluR5 availability in pilocarpine induced epilepsy rat model

mGluR5 expression has been studied using surgical and postmortem specimens in patients as well as in animal models (10-12). However, the findings of these biopsy/autopsy studies could not be referred to when we try to do preoperative clinical evaluation. Recent advances in mGluR5 PET using specific ligands enabled quantitative assessment of receptor availability and its serial noninvasive monitoring (30-32).

In this study, the changes of mGluR5 availability were consistent with previous pathologic studies using *in vitro* techniques in the same pilocarpine-induced epilepsy model. Previous pathologic studies revealedpilocarpine-induced chronic epileptic rats had reduced mGluR5 expression in the hippocampus (11). Furthermore, at 24 h after status epilepticus, mGluR5 expression decreased in amygdala, piriform and entorhinal cortices (12). Our data alsoshowed reduced mGluR5 availability in bilateral hippocampi in chronic epilepsy rat models despite preserved mGluR5 receptor expression in IHC analyses. mGluR5 availability was reduced in the brain globally at 24 h after status epilepticus and this abnormality

persisted in the amygdala and dorsal hippocampus in subacute and chronic periods, though the receptor availability was restored mostly in other areas than hippocampus and amygdala in chronic period. These *in vivo* findings were also corroborated by our IHC analysis which showed globally decreased density of mGluR5 in acute periods. However, IHC analysis revealed no significantly reduced mGluR5 immunoreactivity in the hippocampus of the chronic model.

Pilocarpine-induced status epilepticus is characterized by generalized tonic-clonic seizures. The rats go into a seizure-free period during 2-3 weeks, followed by chronic period with spontaneous seizure activity. Decreased mGluR5 BP_{ND} in acute period after status epilepticus could be associated with postictal status, while that in subacute period might be independent to acute seizure activity because the rats were seizure-free. Thus, temporal changes in mGluR5 BP_{ND} implied gradual molecular changes during epileptogenesis rather than epileptic seizure activity itself.

In acute period after status epilepticus, overactivation of glutamatergic neuron might lead to reduced availability of mGluR5 BP_{ND} in the entire brain. Because of increased glutamate release which occupied more the postsynaptic receptors after pilocarpine-induced long-lasting status epilepticus(84), mGluR5 availability would become globally decreased in acute period. Previous study reported increased glutamate level induced by N-acetylcystein reduced mGluR5 BP_{ND}, though ABP688 is allosteric modulator(85), suggesting that excessive glutamate release

contribute to the reduction of mGluR5 BP_{ND} in acute period.

However, mGluR5 availability measured on [^{11}C]ABP688 PET has a complex relation with mGluR5 expression of the neurons, in that various factors could contribute to the decrease of mGluR5 BP_{ND} in the epileptic rat brain. In the study by Kirschstein, et al., the decrease of mGluR5 expression was mainly caused by down-regulation of receptor molecules in the neurons but they reported that the neuronal cell loss also partially contributed to this decrease (11). Magnetic resonance imaging (MRI) studies also showed progressively decreasing hippocampal volume in the pilocarpine-induced epilepsy model (86, 87). Thus, both volume decrease and down-regulation should be considered when explaining the low [^{11}C]ABP688 binding in hippocampus and amygdala in the chronic period observed in our investigation. By the way, as we found that decreased BP_{ND} of mGluR5 in acute period recovered to normal already in subacute period globally in the brain, which was different from MRI findings of global progressive volume reduction (87),and in chronic period, mGluR5 BP_{ND} recovered in the entire brain except for the focal areas of bilateral amygdala and dorsal hippocampus, we speculate that down-regulation of mGluR5 receptor functional activity explains mostly the decreased BP_{ND} in hippocampus and amygdala in chronic period of pilocarpine-induced epileptic rats.

One of the important issues of cross-sectional molecular studies in epilepsy is whether it underlies the epileptogenesis or result of epileptogenic processes(88). In

this study, the cause of mGluR5 BP_{ND} reduction is unknown and could be a result of epileptogenesis. One of the possible mechanisms of mGluR5 changes was an intrinsic antiepileptic response induced by status epilepticus. As mGluR5 antagonist reduces excitability, the reduction of mGluR5 availability in chronicpilocarpine-induced epilepsy may represent an endogeneousantiepileptic effort(89, 90). This interpretation depends on the previoussuggestion of feedback regulation of excitability related to neuronal homeostasis (91, 92). Alternatively, neuronal network abnormality due to mGluR5 signal reduction would work in chronic period ofpilocarpine-induced epilepsy. Decreased mGluR5 expression induced the reduction of long term depression, thus causing the abnormal activities of the neuronal network in the epileptic brain(11).In genetic autism models, mGluR5 decrease caused network abnormalities(93), where mGluR5 abnormality underlay the pathogenesis of autistic features. Though the causal relationship between mGluR5 changes and epileptogensis is still unclear, the spatial and temporal changes in mGluR5 using [^{11}C]ABP688 PET provided an essential macroscopic functional features of glutamatergic synapses of epileptic rat brain associated with epileptogenesis.

Metabolic brain connectivity

In this study, we obtained interregional metabolic correlations to investigate functional connectivity. Metabolic network analyses could take advantage of the

sequential coupling of neuronal activity, regional brain metabolism and perfusion. Thus, metabolic connectivity abnormality might be observed earlier than that of cerebral blood flow connections (i.e. fMRI or water PET) in progressive brain diseases. Previous studies revealed metabolic connectivity was a sensitive and early diagnostic method in degenerative brain disorders such as Alzheimer's dementia(94-96).

Because metabolic activities measured by PET and fMRI signals reflected different physiologic processes, there is a mismatch between functional networksusing those different modalities(61, 62). Biological signals obtained from two modalities are different, which BOLD signals are contributed by micro- and macrovasculatures(97), whereas FDG uptake depends on metabolic demands in neural tissues. Functional connectivity based on a variation of metabolic demands in this study is distinct from tiny fluctuations of BOLD signals, thus,it could be closer to neuronal energy-activity information(56, 98). BOLD signals indirectly reflect the neuronal activities by measuring a combination of hemodynamic parameters including cerebral blood flow and cerebral blood volume. While widely performed network analyses based on small fluctuations of BOLD signals does not account for baseline neuronal activities which could be the major element, metabolic connectivity constructed by PET reflects directly neuronal energy demands, which could be normalized and adjusted accounting for whole brain activities(56, 98, 99).

Recently, interregional correlation analysis in the rodent brain was performed several times using different imaging modalities or *ex vivo* brain sections. Wang *et al.* used autoradigraphic cerebral perfusion studies to evaluate brain connectivity(100, 101)and Fidalgo*et al.* analyzed brain metabolic connectivity measured by cytochrome oxidase immunohistochemistry(102). To examine interregional correlation using PET images or brain sections, inter-subject correlation was employed. Thus, well-controlled rodent models could have advantages of yielding consistent results with less confounding variables compared to human subject data showing variability of age, gender and other clinical parameters. Various brain disorders including neurodegenerative disease as well as epilepsy can now be evaluated by examining metabolic connectivity in small animals using microPET as a noninvasive imaging tool.

Abnormal brain connections in the epileptic brain

We found significantly weaker connections, particularly involving the left amygdala and left entorhinal cortex in the epilepsy rats. Furthermore, differences in regional graph properties (i.e. decreased nodal and local efficiency) were the highest in the left amygdala, followed by left entorhinal cortex. Of note, these brain structures are important in the pilocarpine-induced epilepsy rat model because histopathologicabnormalities such as injured and degenerating neurons were found in these areas as well as in bilateral hippocampi(103-106). Pilocarpine-induced

epilepsy showed widespread neuronal damage and involved several brain regions(106, 107), which corresponded to the global network disruption found in this study.Moreover, as a neurotransmitter system imaging, we successfully found reduced mGluR5 BP_{ND} in amygdala as well as hippocampus. Histopathological and imaging studies consistently suggested amygdala and limbic-paralimbic structures were culprit lesions.

We found the asymmetric brain network disruption in the epileptic rat brain. To be specific, regional graph theoretic measures were abnormal and connectivity was reduced asymmetrically in the left amygdala and entorhinal cortex in our study, in line with the previous reports. Consistent with the previous EEG data and behavioral features, epileptic discharges were more likely to have initiated in the left hemisphere than in the right hemisphere in the medial TLE patients(108, 109)as well as in the pilocarpine-induced epilepsy rat model(110).

Disrupted network integrity in the epilepsy rats reminded the previous fMRI data from human medial TLE patients(111). The differences in regional graph theoretic measures in the epileptic rat brain implied network disruption, closer to random topology than small-world property. Our results coincided with the previous report of network analysis in the rat model, where the authors found the increase in shortest path length and the decrease in clustering coefficient in experimental focal epilepsy models using fMRI(112). Electrophysiologic data acquired from the rats with glutamate-injured hippocampal neuronal network

showed also the disruption of small-worldness properties(113). In spite of different modalities and animal models, disruption in the network properties in epileptic rat brain has been consistently reported.

The abnormal graph theoretic measures characterized by reduced efficiency have been reported in neurodegenerative disorders such as Alzheimer's dementia(94, 114-116). In chronic medial TLE patients, cognitive impairment is very common and important for neuropsychiatric morbidity(117, 118).Thus, our finding of disrupted network properties in epilepsy rat models similar to neurodegenerative disorders might be related with the global cognitive changes in epilepsy, though the graph theoretic measures are not the hallmarks of brain dysfunction for cognitive impairment. The global network disruption in the epileptic rat brain can be used to explain various neuropsychiatric features, while regional abnormality in brain perfusion or metabolism cannot explain the diverse cognitive symptoms in chronic medial TLE patients, indicating that medial TLE should be considered as a brain network disorder.

Regional metabolic abnormalities in epilepsy

FDG PET in medial TLE patient is a routine workup procedure in the clinical setting. The patients show hypometabolism in mesial temporal lobe, which used to extend to lateral temporal structure(119). Previously, Goffin*et al.* revealed that FDG PET in the chronic pilocarpine epilepsy rat model showed hypometabolism in

left striatum and left entorhinal cortex and hypermetabolism in brainstem and cerebellum(120). There were different results, as Lee *et al.* reported that chronic pilocarpine-induced epilepsy model showed hypometabolism in the entire hippocampi and bilateral amygdala (121)while they compared chronic period of epilepsy and baseline. In our results, epilepsy rats showed significant hypometabolism in cerebral cortex involving anterior cingulate gyrus, bilateral motor cortex, left somatosensory cortex, bilateral anterior hippocampus and left entorhinal cortex (Figure 16, Figure17), using voxel-based T-test with FDR correction ($p< 0.05$, FDR corrected) compared with sham-treated controls. Small region in medulla oblongata showed significant hypermetabolism in the epilepsy model, which was much similar to Goffin's previous result. Hypometabolic regions were not limited to limbic system but involved cerebral cortex, which might be related to the global network abnormality. We found significantly reduced connectivity across cerebral cortical structures as well as limbic systems, suggesting network disruption between limbic system and cortex. We think that this could play a role in yielding cortical hypometabolism. In a kainate-induced chronic epilepsy model, similar to the pilocarpine-induced epilepsy model, hypometabolism was reported in cerebral cortex(122).

Interestingly, the abnormal connectivity found in the network analysis in the present study corresponded, in parts, with regional hypometabolic areas. But, we did not find regional hypometabolism in the left amygdala where the most

significant difference was found on regional graph theoretical measures. We suggest that regional hypometabolism reflect the network abnormalities but do not reflect entirely them. The combined effect of the regional hypometabolism and the network abnormalities associated with or without regional abnormalities should be considered to explain brain dysfunction. Of course, the disrupted interregional connectivity could also be observed without regional abnormalities detected on voxel-based analysis. Therefore, regional and global network parameters could provide functional network abnormalities which were not detected on voxel-based analysis to find regional abnormalities.

Determination of abnormalities of the brain network measures may be useful in the clinical setting because extratemporal abnormalities are closely related to surgical outcome in medial TLE (123, 124).The functional network studies might be used to predict patients' prognosis and to provide correlations of brain network dysfunction with clinical features in the future.

Persistent homology framework for network analysis

We applied a new network modeling method using the persistent homology which Lee et al. reported previously in child patients with autism spectrum disorder and attention-deficit hyperactivity disorder(67). To avoid using arbitrary thresholds to make binary networks, we applied all the possible thresholds to the interregional correlation matrices and found that the networks could be summarized by the

subsets of the Rips complex. Multiscale networks were produced for each group and visualized by dendrogram. Single linkage matrix was the equivalent representation of single linkage dendrogram. Upon our analysis, single linkage matrix comparison between epilepsy rats and controls showed a tendency of weak connection involving left insular cortex as well as left amygdala, though the difference did not reach statistical significance after multiple comparison correction. Of note, insular cortex played an important role in medial TLE, which mediated the spreading of epileptic activity and surgical ablation of the insular cortex reduced seizure activities(125-127). Pilocarpine-induced status epilepticus caused interneuron loss in insular cortex(128)and insular cortex was regarded as a hub in the progression of epileptic discharges in patients with medial TLE (129). Therefore, not only left amygdala and entorhinal cortex, but insular cortex could have played roles in epileptic network disruption, suggesting a limbic-paralimbic (i.e. insula and entorhinal cortex)-neocortical connection abnormality in the epileptic rat brain.

A direct comparison of metabolic network and graph theoretic measures showed abnormal connectionsinvolving left amygdala. The findings of persistent homology brain network analyses partly corresponded to direct comparison. However, while direct connectivity comparisons (i.e. comparison of c_X) reflected covariance patterns of only two nodes, persistent homology framework could provide functional distance of nodes after generating a global brain network, a

status of all nodes were connected. The connected component might reflect how information merged and shared across all the nodes. Thus, a tendency of weak connections found in persistent homology framework enlighten where delayed information flow happen in epilepsy. In this aspect, left insular cortex, where direct comparisons and graph theoretic measures analyses did not significantly find, is additionally found as an important region in epilepsy, which correspond to a hub of epileptic discharge in human TLE (129).

In short, we successfully found dysfunctional brain networks in the epileptic rat brain. We showed that the most significant connections in the epilepsy rat models involved the left amygdala and left entorhinal cortex. These areas showed significant changes in the epileptic rat group on graph theoretic measures. Furthermore, SLD increased in the connectomes between left insular cortex/amygdala and cortical/subcortical structures, which implied abnormally connected network in epilepsy rat brain. Our approaches including direct connectivity comparison, graph theoretic measures, and persistent brain homology-based single linkage matrix consistently showed abnormal connections in the left limbic-paralimbic-neocortical network in the epileptic rat brain.

Functional connectivity in mGluR5 associated regions

We revealed reduced connectivity inmGluR5 associated networksin epilepsy. Functional brain networks are mediated by neurotransmittersin synapse. However,

those molecular level changes have been difficult to be interpreted by global systematic changes. Besides, microscopic synaptic molecular changes could not explain behavioral and systematic functions.

Microscopic synaptic changes in mGluR5 could affect neuronal connectivity and dynamics (70, 130). Our findings of mGluR5 associated regions with reduced metabolic connectivity were consistent with the previous finding that mGluR5 agonist enhanced neuronal coactivation(70, 71).Considering recently developed mGluR5-targeted drugs for autism and Fragile X syndrome (28, 93, 131), receptor related molecular dynamics affect global brain network which may cause behavioral improvement (93). Because several drugs for neuropsychiatric disorders targeted neurotransmitters, comprehensive approaches are warranted to link mechanisms of molecular changes and global brain connectome.

In this study, we introduced a novel approach for global effects of neurotransmitter changes using interregional network analyses. Up to date, a PET study suggested a relationship between different neurotransmitter systems by multifunctional connectivity approach (132). [^{11}C]ABP688 PET revealed significant regions in the epilepsy models, thus we speculated those regions could be functionally associated though they were anatomically separated from each other. In controls, metabolic covariance of mGluR5 associated regions were concurrent (i.e. correlation coefficients were more than 0.94 for all pairwise clusters), which suggested the regions were functionally relevant. Reminded by

significantly reduced mGluR5 BP_{ND} in those clusters, we speculated there are mGluR5-associated networks and the networks are functionally connected to each other. In the epilepsy models, metabolic covariance patterns were asynchronous and their connectivitywas markedly reduced. As the global network analyses revealed limbic-paralimbic-neocortical network disruption, mGluR5 associated networks were found in focal regions of limbic-paralimbic structures which had markedly reduced functional connectivity.

To analyze large-scale functional connectivity, the manner how to define nodes of network is important. Anatomically defined regions are usually used though they have limitation in functional information. We selected four small clusters where mGluR5 abnormality was found, which provided the specific neurotransmitter system based components. In spite of the significant abnormal connectivity, causal relationship of mGluR5 remains unknown. Furthermore, because neural circuits are heavily connected to each other across entire brain, functional correlations in the small clusters are hard to reflect brain network abnormality.

In the future, multifunctional and multimodal imaging analyses promise to construct multidimensional functional connectomeaccording to molecular level changes. Because multiple neurotransmitter systems interplay and make brain functions, our approach could provide etiological molecular changes and their interconnections. Furthermore, using our approaches, an image-based biomarker could be developed with comprehensive etiological background and evaluateeffects

of new therapeutics for brain disorders.

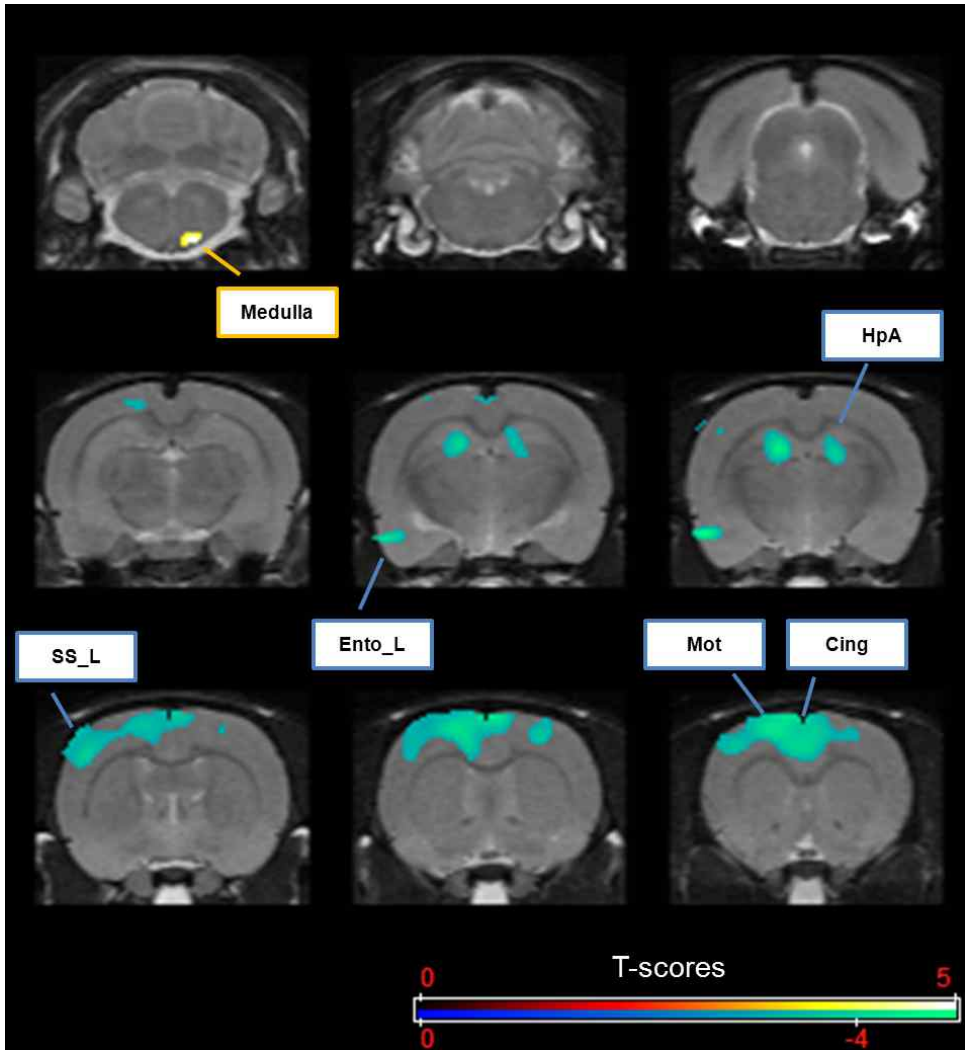
Medulla
HpA
SS_L
Ento_L
Mot
Cing
T-scores
0
5
0
-4

FIGURE 16.Comparison of brain metabolism between epilepsy models and controls using voxel-based analysis. Brain metabolic activity was globally normalized, and we performed voxel-by-voxel comparison using statistical parametric mapping (SPM2). To identify significant voxels, we applied FDR corrected $q < 0.05$ as a threshold and extent threshold $k = 100$. Epilepsy models showed significant hypometabolism in cerebral cortex involving anterior cingulate gyrus, bilateral motor cortex, left somatosensory cortex as well as bilateral anterior hippocampus and left entorhinal cortex. Statistically significant hypermetabolism in models were found in medulla oblongata.

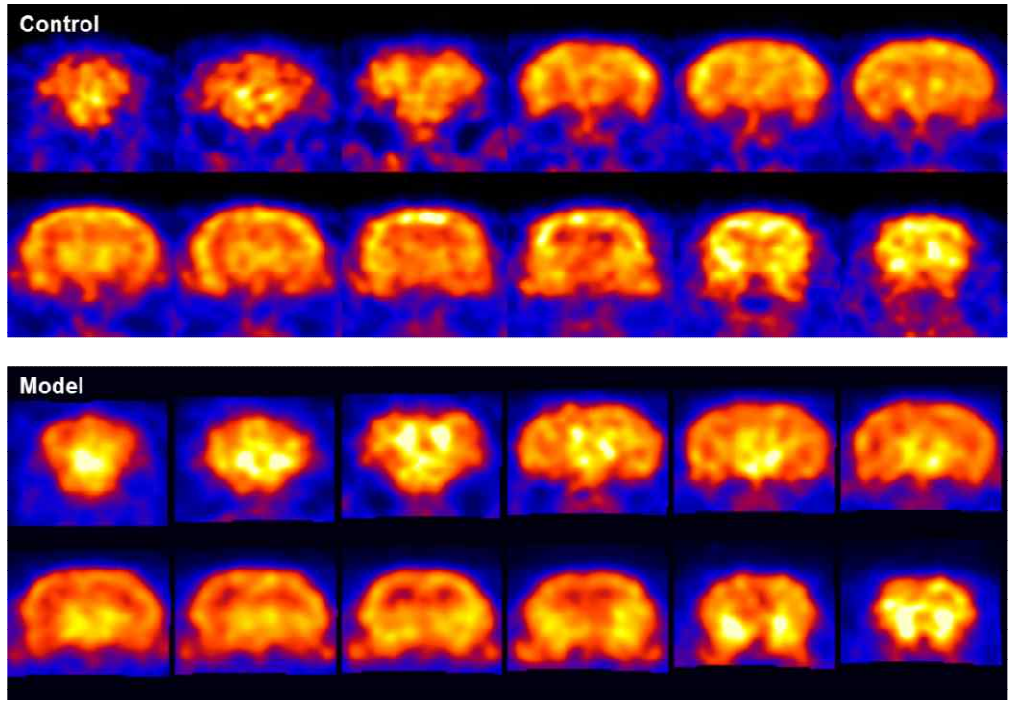

FIGURE 17.Representative PET images of epilepsy models and controls.

Limitation and Further Study

As a first experiment, we studied the temporal changes in mGluR5 BP_{ND} after status epilepticus, however, the controls were only assessed at chronic periods, not at all the time points. Repeated anesthesia and imaging was difficult for seriously ill epileptic rats, though. Temporal patterns of mGluR5 BP_{ND} changes were not exactly paired and individual variation between unpaired data would have obliterated the subtle differences between groups or changes within groups. Despite this limitation, however, the results showed prominent temporal changes of BP_{ND} through the acute and subacute periods and finally in chronic period. We used ^{11}C-labeled compound, thus, relatively short physical half-life compared with ^{18}F-labeled compound was disadvantage in clinical application. However, compared to recently developed [^{18}F]FPEB, [^{11}C]ABP688 has advantages in well-established kinetics and receptor-ligand properties (33, 36, 133). Several mGluR5 targeted tracers including [^{18}F]FPEB could be used to estimate mGluR5 availability in the future (36, 133).

[^{11}C]ABP688 PET promises us to evaluate the mGluR5 changes during epileptogenesis and pathogenesis of neurological diseases. Because [^{11}C]ABP688 PET was already used in patients with neurological and psychiatric disorders(32), we propose that [^{11}C]ABP688 PET be used in epilepsy patients hopefully to find seizure focus as well as to evaluate the progress of pathophysiology of epilepsy. Being reminded by the report that mGluR5 expression did not decrease but

increase in the hippocampus in medial TLE patients (11), [^{11}C]ABP688PET findings should be interpreted comprehensively because they reflected the mixture of primary pathology and compensatory changes of the human brain to epileptogenesis. [^{11}C]ABP688 PET might enlighten us in classifying seizure disorders in a refined fashion in terms of glutamatergic neurotransmission during pathophysiologic progress of intractable medial temporal lobe epilepsy in human as well as in rat models.

In our study, because the purpose was to evaluate *in vivo* mGluR5 availability and metabolic connectivity changes in epilepsy models, neither EEG monitoring of the rats nor frequency of spontaneous recurrent seizures was documented. mGluR5 imaging correlated with clinical features may provide functional grading and classification for TLE. Moreover, to elucidate mGluR5 associated pathophysiology of epilepsy and to speculate its role in spontaneous seizure, the relationship between disease severity and mGluR5 availability patterns should be investigated as a future work. Functional connectivity abnormalities could be also related to seizure severity, thus, the relationship between symptom and metabolic connectivity needs to be clarified to find which connections were important for spontaneous seizures and seizure severity.

The most important clinical manifestation of epilepsy is spontaneous recurrent seizure. However, what mainly causes the spontaneous neuronal excitation is still unknown. Several neurotransmitter systems including mGluR5 related

glutamatergic changes and their complex networks may underlieepileptogenesis(134-136).However, our findings including mGluR5 changes and metabolic connectivity disruptions in chronic epilepsy rat models are disease related findings, not underlying pathogenesis. As we discussed before, for epilepsy research, cross-sectional studies are unable to differentiate underlying pathophysiology from the results of epileptogenic process. Metabolic connectivity abnormalities in our results could be partly associated with the neuronal homeostasis (90, 91), a feedback regulation of excitability to reduce hyperexcitability. Thus, the network abnormality in epilepsy, what we could find with imaging and histologic studies, may be a mixture of causal and results of neuronal hyperexcitation. In the future, a well-controlled animal study will provide hints for the differentiating them. Specifically, the pilocarpine-induced epilepsy rat models can be modulated by pilocarpine dose and the duration of status epilepticus(107). These approaches can classify theanimals according to the severity of status epilepticus and the existence of spontaneous seizure. Molecular and network patterns associated with those features will provide what abnormalities may underlie epileptogenesis.

In our study, for quantitative analysis for mGluR5, dynamic scans started from injection were needed. So, the animals were anesthetized during [^{11}C]ABP688 PET acquisition. Isoflurane was used for inhalation anesthesia in this study. The mechanism of action of inhalation anesthesia remains still incompletely understood,

while isoflurane bind to GABA, glutamate and glycine receptors of brain (137, 138). Furthermore, to our knowledge, there is no report that inhalation anesthesia is directly related to mGluR5. However, intravenous anesthesia such as ketamine is modulated by mGluR5 (139). Since N-methyl-D-aspartate (NMDA) receptor function, a target receptor for several intravenous drugs for anesthesia, is changed by mGluR1 and mGluR5 induced synaptic plasticity, those receptors density in the brain during anesthesia may be changed. Though it was inevitable to use anesthesia during [^{11}C]ABP688 PET acquisition, the effects of it change mGluR5 availability. Nevertheless, both controls and the rat models were scanned with same protocol, so, both the animals might be similarly affected by anesthesia even if isoflurane bound to mGluR5 which affected results of PET quantification. For metabolic connectivity experiment, the rats were awake during FDG uptake period, followed by static PET acquisition under anesthesia. Since animalsare anesthetized after the uptake of FDG by the brain,our protocolcan measure brain metabolism in awakerats. This awake PET protocol is possible when quantification parameters of static PET scans (*e.g.* Standardized uptake value, SUV) can be used as alternative parameters for dynamic PET based quantification. If static [^{11}C]ABP688 PET scans allow us to calculate a parameter closely correlated with BP_{ND} obtained from dynamic PET scans, we can assess mGluR5 density with minimized anesthesia effects.

Pilocarpine induced epilepsy rat model has a feature of pharmacoresistance.

Previous studies suggest that effluxtransporters such as P-glycoprotein (Pgp) at the blood–brain barrier (BBB) areimportant for pharmacoresistance. These mechanisms reduce the concentration of antiepileptic drugs in the brain and contributing to drug resistance(140). Since wide range of drugs are substrates for Pgp and transporter proteins at BBB, PET tracers including FDG and [^{11}C]ABP688 may partly be altered by the transporters activity. Although receptors are not changed by the transporters, tissue influx and efflux mechanism are altered by transporters at BBB, which eventually affect the estimation of PET parameters such as BP_{ND}. To investigate that mGluR5 receptor binding of [^{11}C]ABP688 can be altered by the transporters at BBB, mGluR5 BP_{ND} estimation can be investigated in the epilepsy rat model whenPgp protein inhibitors such as tarquida are treated. One of the widely used radioligands for epilepsy, [^{11}C]flumazenil for $GABA_A$ receptor was studied whether Pgp inhibition alter the GABA receptor binding in kainite induced epilepsy rat model(141). Moreover, using PET tracers substrates for Pgp provide quantitative efflux activity at BBB in epilepsy rat model(142). Combined measurement of BBB efflux activity and other PET imaging agents will allowcomprehensive analyses for pharmacokinetics in epilepsy rat model.

Conclusion

We demonstrated that abnormal mGluR5 availability and metabolic connectivity in the pilocarpine-induced epilepsy rat models. Not only were regional glutamate systems but metabolic correlation significantly different between the epilepsy rats and controls, particularly involving limbic-paralimbic networks. Furthermore, brain network modeling and the topological properties could provide functional connectivity abnormalities. Functional connectivity was disrupted particularly in mGluR5-associated network. Our results from small-animal models suggest that functional brain network analysis could be applied to the preclinical studies using rat brain models to yield the hallmarks of various human brain disorders.

References

1. Spencer SS. Neural networks in human epilepsy: evidence of and implications for treatment. Epilepsia. 2002;43:219-27.

2. Blumenfeld H, McNally KA, Vanderhill SD, Paige AL, Chung R, Davis K, et al. Positive and negative network correlations in temporal lobe epilepsy. Cereb Cortex. 2004;14:892-902.

3. Ure J, Baudry M, Perassolo M. Metabotropic glutamate receptors and epilepsy. J Neurol Sci. 2006;247:1-9.

4. Doherty J, Dingledine R. The roles of metabotropic glutamate receptors in seizures and epilepsy. Curr Drug Targets CNS Neurol Disord. 2002;1:251-60.

5. Bianchi R, Wong RKS, Merlin LR. Glutamate Receptors in Epilepsy: Group I mGluR-Mediated Epileptogenesis. In: Noebels JL, Avoli M, Rogawski MA, Olsen RW, Delgado-Escueta AV, editors. Jasper's Basic Mechanisms of the Epilepsies. 4th ed. Bethesda (MD)2012.

6. Watabe AM, Carlisle HJ, O'Dell TJ. Postsynaptic induction and presynaptic expression of group 1 mGluR-dependent LTD in the hippocampal CA1 region. J Neurophysiol. 2002;87:1395-403.

7. Merlin LR. Differential roles for mGluR1 and mGluR5 in the persistent prolongation of epileptiform bursts. J Neurophysiol. 2002;87:621-5.

8. Aronica E, Gorter JA, Jansen GH, van Veelen CW, van Rijen PC, Ramkema M, et al. Expression and cell distribution of group I and group II

metabotropic glutamate receptor subtypes in taylor-type focal cortical dysplasia. Epilepsia. 2003;44:785-95.

9. Blumcke I, Becker AJ, Klein C, Scheiwe C, Lie AA, Beck H, et al. Temporal lobe epilepsy associated up-regulation of metabotropic glutamate receptors: correlated changes in mGluR1 mRNA and protein expression in experimental animals and human patients. J Neuropathol Exp Neurol. 2000;59:1-10.

10. Notenboom RG, Hampson DR, Jansen GH, van Rijen PC, van Veelen CW, van Nieuwenhuizen O, et al. Up-regulation of hippocampal metabotropic glutamate receptor 5 in temporal lobe epilepsy patients. Brain. 2006;129:96-107.

11. Kirschstein T, Bauer M, Muller L, Ruschenschmidt C, Reitze M, Becker AJ, et al. Loss of metabotropic glutamate receptor-dependent long-term depression via downregulation of mGluR5 after status epilepticus. J Neurosci. 2007;27:7696-704.

12. Cavarsan CF, Tescarollo F, Tesone-Coelho C, Morais RL, Motta FL, Blanco MM, et al. Pilocarpine-induced status epilepticus increases Homer1a and changes mGluR5 expression. Epilepsy Res. 2012;101:253-60.

13. Enz R. Metabotropic glutamate receptors and interacting proteins: evolving drug targets. Curr Drug Targets. 2012;13:145-56.

14. Cartmell J, Schoepp DD. Regulation of neurotransmitter release by metabotropic glutamate receptors. J Neurochem. 2000;75:889-907.

15. Braunewell KH, Manahan-Vaughan D. Long-term depression: a cellular basis for learning? Rev Neurosci. 2001;12:121-40.

16. Luscher C, Huber KM. Group 1 mGluR-dependent synaptic long-term depression: mechanisms and implications for circuitry and disease. Neuron. 2010;65:445-59.

17. Oddo S, Caccamo A, Shepherd JD, Murphy MP, Golde TE, Kayed R, et al. Triple-transgenic model of Alzheimer's disease with plaques and tangles: intracellular Abeta and synaptic dysfunction. Neuron. 2003;39:409-21.

18. Beck H, Goussakov IV, Lie A, Helmstaedter C, Elger CE. Synaptic plasticity in the human dentate gyrus. J Neurosci. 2000;20:7080-6.

19. Williams SC. Drugs targeting mGluR5 receptor offer 'fragile' hope for autism. Nat Med. 2012;18:840.

20. Ronesi JA, Collins KA, Hays SA, Tsai NP, Guo W, Birnbaum SG, et al. Disrupted Homer scaffolds mediate abnormal mGluR5 function in a mouse model of fragile X syndrome. Nat Neurosci. 2012;15:431-40, S1.

21. Jacquemont S, Curie A, des Portes V, Torrioli MG, Berry-Kravis E, Hagerman RJ, et al. Epigenetic modification of the FMR1 gene in fragile X syndrome is associated with differential response to the mGluR5 antagonist AFQ056. Sci Transl Med. 2011;3:64ra1.

22. Sokol DK, Maloney B, Long JM, Ray B, Lahiri DK. Autism, Alzheimer disease, and fragile X: APP, FMRP, and mGluR5 are molecular links. Neurology.

2011;76:1344-52.

23. Seese RR, Maske AR, Lynch G, Gall CM. Long-Term Memory Deficits are Associated with Elevated Synaptic ERK1/2 Activation and Reversed by mGluR5 Antagonism in an Animal Model of Autism. Neuropsychopharmacology. 2014;39:1664-73.

24. Bear MF, Huber KM, Warren ST. The mGluR theory of fragile X mental retardation. Trends Neurosci. 2004;27:370-7.

25. Dolen G, Bear MF. Role for metabotropic glutamate receptor 5 (mGluR5) in the pathogenesis of fragile X syndrome. J Physiol. 2008;586:1503-8.

26. Ametamey SM, Kessler LJ, Honer M, Wyss MT, Buck A, Hintermann S, et al. Radiosynthesis and preclinical evaluation of ^{11}C-ABP688 as a probe for imaging the metabotropic glutamate receptor subtype 5. J Nucl Med. 2006;47:698-705.

27. Gasparini F, Lingenhohl K, Stoehr N, Flor PJ, Heinrich M, Vranesic I, et al. 2-Methyl-6-(phenylethynyl)-pyridine (MPEP), a potent, selective and systemically active mGlu5 receptor antagonist. Neuropharmacology. 1999;38:1493-503.

28. Silverman JL, Tolu SS, Barkan CL, Crawley JN. Repetitive self-grooming behavior in the BTBR mouse model of autism is blocked by the mGluR5 antagonist MPEP. Neuropsychopharmacology. 2010;35:976-89.

29. Suvrathan A, Hoeffer CA, Wong H, Klann E, Chattarji S. Characterization

and reversal of synaptic defects in the amygdala in a mouse model of fragile X syndrome. Proc Natl Acad Sci U S A. 2010;107:11591-6.

30. Deschwanden A, Karolewicz B, Feyissa AM, Treyer V, Ametamey SM, Johayem A, et al. Reduced metabotropic glutamate receptor 5 density in major depression determined by [^{11}C]ABP688 PET and postmortem study. Am J Psychiatry. 2011;168:727-34.

31. Akkus F, Ametamey SM, Treyer V, Burger C, Johayem A, Umbricht D, et al. Marked global reduction in mGluR5 receptor binding in smokers and ex-smokers determined by [^{11}C]ABP688 positron emission tomography. Proc Natl Acad Sci U S A. 2013;110:737-42.

32. Ametamey SM, Treyer V, Streffer J, Wyss MT, Schmidt M, Blagoev M, et al. Human PET studies of metabotropic glutamate receptor subtype 5 with ^{11}C-ABP688. J Nucl Med. 2007;48:247-52.

33. Elmenhorst D, Minuzzi L, Aliaga A, Rowley J, Massarweh G, Diksic M, et al. In vivo and in vitro validation of reference tissue models for the mGluR(5) ligand [^{11}C]ABP688. J Cereb Blood Flow Metab. 2010;30:1538-49.

34. Mintun MA, Raichle ME, Kilbourn MR, Wooten GF, Welch MJ. A quantitative model for the in vivo assessment of drug binding sites with positron emission tomography. Ann Neurol. 1984;15:217-27.

35. Lammertsma AA, Hume SP. Simplified reference tissue model for PET receptor studies. Neuroimage. 1996;4:153-8.

36. Wong DF, Waterhouse R, Kuwabara H, Kim J, Brasic JR, Chamroonrat W, et al. ^{18}F-FPEB, a PET radiopharmaceutical for quantifying metabotropic glutamate 5 receptors: a first-in-human study of radiochemical safety, biokinetics, and radiation dosimetry. J Nucl Med. 2013;54:388-96.

37. Sobrio F. Radiosynthesis of carbon-11 and fluorine-18 labelled radiotracers to image the ionotropic and metabotropic glutamate receptors. J Labelled Comp Radiopharm. 2013;56:180-6.

38. Braakman HM, van der Kruijs SJ, Vaessen MJ, Jansen JF, Debeij-van Hall MH, Vles JS, et al. Microstructural and functional MRI studies of cognitive impairment in epilepsy. Epilepsia. 2012;53:1690-9.

39. Vlooswijk MC, Jansen JF, Majoie HJ, Hofman PA, de Krom MC, Aldenkamp AP, et al. Functional connectivity and language impairment in cryptogenic localization-related epilepsy. Neurology. 2010;75:395-402.

40. la Fougere C, Rominger A, Forster S, Geisler J, Bartenstein P. PET and SPECT in epilepsy: a critical review. Epilepsy Behav. 2009;15:50-5.

41. Lee DS, Lee SK, Lee MC. Functional neuroimaging in epilepsy: FDG PET and ictal SPECT. J Korean Med Sci. 2001;16:689-96.

42. Lee SK, Lee SY, Yun CH, Lee HY, Lee JS, Lee DS. Ictal SPECT in neocortical epilepsies: clinical usefulness and factors affecting the pattern of hyperperfusion. Neuroradiology. 2006;48:678-84.

43. Lee JJ, Kang WJ, Lee DS, Lee JS, Hwang H, Kim KJ, et al. Diagnostic

performance of ^{18}F-FDG PET and ictal ^{99m}Tc-HMPAO SPET in pediatric temporal lobe epilepsy: quantitative analysis by statistical parametric mapping, statistical probabilistic anatomical map, and subtraction ictal SPET. Seizure. 2005;14:213-20.

44. Voets NL, Beckmann CF, Cole DM, Hong S, Bernasconi A, Bernasconi N. Structural substrates for resting network disruption in temporal lobe epilepsy. Brain. 2012;135:2350-7.

45. Bettus G, Guedj E, Joyeux F, Confort-Gouny S, Soulier E, Laguitton V, et al. Decreased basal fMRI functional connectivity in epileptogenic networks and contralateral compensatory mechanisms. Hum Brain Mapp. 2009;30:1580-91.

46. Liao W, Zhang Z, Pan Z, Mantini D, Ding J, Duan X, et al. Altered functional connectivity and small-world in mesial temporal lobe epilepsy. PLoS One. 2010;5:e8525.

47. Bernhardt BC, Chen Z, He Y, Evans AC, Bernasconi N. Graph-theoretical analysis reveals disrupted small-world organization of cortical thickness correlation networks in temporal lobe epilepsy. Cereb Cortex. 2011;21:2147-57.

48. Sequeira KM, Tabesh A, Sainju RK, DeSantis SM, Naselaris T, Joseph JE, et al. Perfusion network shift during seizures in medial temporal lobe epilepsy. PLoS One. 2013;8:e53204.

49. Trotta N, Goldman S, Legros B, Baete K, Van Laere K, Van Bogaert P, et al. Changes in functional integration with the non-epileptic temporal lobe of patients with unilateral mesiotemporal epilepsy. PLoS One. 2013;8:e67053.

50. Friston KJ, Frith CD, Liddle PF, Frackowiak RS. Functional connectivity: the principal-component analysis of large (PET) data sets. J Cereb Blood Flow Metab. 1993;13:5-14.

51. Horwitz B. The elusive concept of brain connectivity. Neuroimage. 2003;19:466-70.

52. Shmuel A, Leopold DA. Neuronal correlates of spontaneous fluctuations in fMRI signals in monkey visual cortex: Implications for functional connectivity at rest. Hum Brain Mapp. 2008;29:751-61.

53. Hertz L, Zielke HR. Astrocytic control of glutamatergic activity: astrocytes as stars of the show. Trends in Neurosciences. 2004;27:735-43.

54. Herman P, Sanganahalli BG, Blumenfeld H, Hyder F. Cerebral oxygen demand for short-lived and steady-state events. J Neurochem. 2009;109 Suppl 1:73-9.

55. Aubert A, Costalat R. A model of the coupling between brain electrical activity, metabolism, and hemodynamics: application to the interpretation of functional neuroimaging. Neuroimage. 2002;17:1162-81.

56. Hyder F, Fulbright RK, Shulman RG, Rothman DL. Glutamatergic function in the resting awake human brain is supported by uniformly high oxidative energy. J Cereb Blood Flow Metab. 2013;33:339-47.

57. Horwitz B, Rumsey JM, Grady CL, Rapoport SI. The cerebral metabolic landscape in autism. Intercorrelations of regional glucose utilization. Arch Neurol.

1988;45:749-55.

58. Kang E, Lee DS, Lee JS, Kang H, Hwang CH, Oh SH, et al. Developmental hemispheric asymmetry of interregional metabolic correlation of the auditory cortex in deaf subjects. Neuroimage. 2003;19:777-83.

59. Vogt BA, Vogt L, Laureys S. Cytology and functionally correlated circuits of human posterior cingulate areas. Neuroimage. 2006;29:452-66.

60. Lee DS, Kang H, Kim H, Park H, Oh JS, Lee JS, et al. Metabolic connectivity by interregional correlation analysis using statistical parametric mapping (SPM) and FDG brain PET; methodological development and patterns of metabolic connectivity in adults. Eur J Nucl Med Mol Imaging. 2008;35:1681-91.

61. Di X, Biswal BB, Alzheimer's Disease Neuroimaging I. Metabolic brain covariant networks as revealed by FDG-PET with reference to resting-state fMRI networks. Brain Connect. 2012;2:275-83.

62. Wehrl HF, Hossain M, Lankes K, Liu CC, Bezrukov I, Martirosian P, et al. Simultaneous PET-MRI reveals brain function in activated and resting state on metabolic, hemodynamic and multiple temporal scales. Nat Med. 2013;19:1184-9.

63. Bullmore E, Sporns O. Complex brain networks: graph theoretical analysis of structural and functional systems. Nat Rev Neurosci. 2009;10:186-98.

64. van Wijk BC, Stam CJ, Daffertshofer A. Comparing brain networks of different size and connectivity density using graph theory. PLoS One. 2010;5:e13701.

65. Fornito A, Zalesky A, Breakspear M. Graph analysis of the human connectome: promise, progress, and pitfalls. Neuroimage. 2013;80:426-44.

66. Barabasi AL. Scale-Free Networks: A Decade and Beyond. Science. 2009;325:412-3.

67. Lee H, Kang H, Chung MK, Kim BN, Lee DS. Persistent brain network homology from the perspective of dendrogram. IEEE Trans Med Imaging. 2012;31:2267-77.

68. Carlsson G, Zomorodian A, Collins A, Guibas L, editors. Persistence barcodes for shapes. Proceedings of the 2004 Eurographics/ACM SIGGRAPH symposium on Geometry processing; 2004: ACM.

69. Hays SA, Huber KM, Gibson JR. Altered neocortical rhythmic activity states in Fmr1 KO mice are due to enhanced mGluR5 signaling and involve changes in excitatory circuitry. J Neurosci. 2011;31:14223-34.

70. Zhang F, Liu B, Lei Z, Wang JH. mGluR(1),5 activation improves network asynchrony and GABAergic synapse attenuation in the amygdala: implication for anxiety-like behavior in DBA/2 mice. Mol Brain. 2012;5:20.

71. Lanneau C, Harries MH, Ray AM, Cobb SR, Randall A, Davies CH. Complex interactions between mGluR1 and mGluR5 shape neuronal network activity in the rat hippocampus. Neuropharmacology. 2002;43:131-40.

72. Racine R, Okujava V, Chipashvili S. Modification of seizure activity by electrical stimulation. 3. Mechanisms. Electroencephalogr Clin Neurophysiol.

1972;32:295-9.

73. Lee HJ, Jeong JM, Lee YS, Kim HW, J.Y. C, Lee DS, et al. A convenient radiolabeling of [^{11}C](R)-PK11195 using loop method in automatic synthesis module. Nucl Med Mol Imaging. 2009;43:337-43.

74. Liu X, Comtat C, Michel C, Kinahan P, Defrise M, Townsend D. Comparison of 3-D reconstruction with 3D-OSEM and with FORE+OSEM for PET. IEEE Trans Med Imaging. 2001;20:804-14.

75. Schiffer WK, Mirrione MM, Biegon A, Alexoff DL, Patel V, Dewey SL. Serial microPET measures of the metabolic reaction to a microdialysis probe implant. J Neurosci Methods. 2006;155:272-84.

76. Innis RB, Cunningham VJ, Delforge J, Fujita M, Gjedde A, Gunn RN, et al. Consensus nomenclature for in vivo imaging of reversibly binding radioligands. J Cereb Blood Flow Metab. 2007;27:1533-9.

77. Schiffer WK, Mirrione MM, Dewey SL. Optimizing experimental protocols for quantitative behavioral imaging with ^{18}F-FDG in rodents. J Nucl Med. 2007;48:277-87.

78. Toga AW, Santori EM, Hazani R, Ambach K. A 3D digital map of rat brain. Brain Res Bull. 1995;38:77-85.

79. Haxby JV, Gobbini MI, Furey ML, Ishai A, Schouten JL, Pietrini P. Distributed and overlapping representations of faces and objects in ventral temporal cortex. Science. 2001;293:2425-30.

80. Kriegeskorte N, Mur M, Ruff DA, Kiani R, Bodurka J, Esteky H, et al. Matching categorical object representations in inferior temporal cortex of man and monkey. Neuron. 2008;60:1126-41.

81. Kaiser M. A tutorial in connectome analysis: topological and spatial features of brain networks. Neuroimage. 2011;57:892-907.

82. Latora V, Marchiori M. Efficient behavior of small-world networks. Physical Review Letters. 2001;87.

83. Achard S, Bullmore E. Efficiency and cost of economical brain functional networks. PLoS Comput Biol. 2007;3:e17.

84. Costa MS, Rocha JB, Perosa SR, Cavalheiro EA, Naffah-Mazzacoratti Mda G. Pilocarpine-induced status epilepticus increases glutamate release in rat hippocampal synaptosomes. Neurosci Lett. 2004;356:41-4.

85. Miyake N, Skinbjerg M, Easwaramoorthy B, Kumar D, Girgis RR, Xu X, et al. Imaging changes in glutamate transmission in vivo with the metabotropic glutamate receptor 5 tracer [^{11}C] ABP688 and N-acetylcysteine challenge. Biol Psychiatry. 2011;69:822-4.

86. Niessen HG, Angenstein F, Vielhaber S, Frisch C, Kudin A, Elger CE, et al. Volumetric magnetic resonance imaging of functionally relevant structural alterations in chronic epilepsy after pilocarpine-induced status epilepticus in rats. Epilepsia. 2005;46:1021-6.

87. Nairismagi J, Pitkanen A, Kettunen MI, Kauppinen RA, Kubova H. Status

epilepticus in 12-day-old rats leads to temporal lobe neurodegeneration and volume reduction: a histologic and MRI study. Epilepsia. 2006;47:479-88.

88. Merlin LR. The ups and downs of hippocampal metabotropic glutamate receptors: ramifications for epileptogenesis and cognitive impairment following status epilepticus. Epilepsy Curr. 2008;8:43-5.

89. Tang FR, Chen PM, Tang YC, Tsai MC, Lee WL. Two-methyl-6-phenylethynyl-pyridine (MPEP), a metabotropic glutamate receptor 5 antagonist, with low doses of MK801 and diazepam: a novel approach for controlling status epilepticus. Neuropharmacology. 2007;53:821-31.

90. Lojkova-Janeckova D, Ng J, Mares P. Antagonists of group I metabotropic glutamate receptors and cortical afterdischarges in immature rats. Epilepsia. 2009;50:2123-9.

91. Ramocki MB, Zoghbi HY. Failure of neuronal homeostasis results in common neuropsychiatric phenotypes. Nature. 2008;455:912-8.

92. Sakagami Y, Yamamoto K, Sugiura S, Inokuchi K, Hayashi T, Kato N. Essential roles of Homer-1a in homeostatic regulation of pyramidal cell excitability: a possible link to clinical benefits of electroconvulsive shock. Eur J Neurosci. 2005;21:3229-39.

93. Auerbach BD, Osterweil EK, Bear MF. Mutations causing syndromic autism define an axis of synaptic pathophysiology. Nature. 2011;480:63-8.

94. Seo EH, Lee DY, Lee JM, Park JS, Sohn BK, Lee DS, et al. Whole-brain

functional networks in cognitively normal, mild cognitive impairment, and Alzheimer's disease. PLoS One. 2013;8:e53922.

95. Morbelli S, Drzezga A, Perneczky R, Frisoni GB, Caroli A, van Berckel BN, et al. Resting metabolic connectivity in prodromal Alzheimer's disease. A European Alzheimer Disease Consortium (EADC) project. Neurobiol Aging. 2012;33:2533-50.

96. Toussaint PJ, Perlbarg V, Bellec P, Desarnaud S, Lacomblez L, Doyon J, et al. Resting state FDG-PET functional connectivity as an early biomarker of Alzheimer's disease using conjoint univariate and independent component analyses. Neuroimage. 2012;63:936-46.

97. Yu X, Glen D, Wang S, Dodd S, Hirano Y, Saad Z, et al. Direct imaging of macrovascular and microvascular contributions to BOLD fMRI in layers IV-V of the rat whisker-barrel cortex. Neuroimage. 2012;59:1451-60.

98. Hyder F, Herman P, Sanganahalli BG, Coman D, Blumenfeld H, Rothman DL. Role of ongoing, intrinsic activity of neuronal populations for quantitative neuroimaging of functional magnetic resonance imaging-based networks. Brain Connect. 2011;1:185-93.

99. Smith AJ, Blumenfeld H, Behar KL, Rothman DL, Shulman RG, Hyder F. Cerebral energetics and spiking frequency: the neurophysiological basis of fMRI. Proc Natl Acad Sci U S A. 2002;99:10765-70.

100. Wang Z, Bradesi S, Charles JR, Pang RD, Maarek JM, Mayer EA, et al.

Functional brain activation during retrieval of visceral pain-conditioned passive avoidance in the rat. Pain. 2011;152:2746-56.

101. Wang Z, Pang RD, Hernandez M, Ocampo MA, Holschneider DP. Anxiolytic-like effect of pregabalin on unconditioned fear in the rat: an autoradiographic brain perfusion mapping and functional connectivity study. Neuroimage. 2012;59:4168-88.

102. Fidalgo C, Conejo NM, Gonzalez-Pardo H, Arias JL. Cortico-limbic-striatal contribution after response and reversal learning: a metabolic mapping study. Brain Res. 2011;1368:143-50.

103. Turski WA, Cavalheiro EA, Schwarz M, Czuczwar SJ, Kleinrok Z, Turski L. Limbic seizures produced by pilocarpine in rats: behavioural, electroencephalographic and neuropathological study. Behav Brain Res. 1983;9:315-35.

104. Wozny C, Gabriel S, Jandova K, Schulze K, Heinemann U, Behr J. Entorhinal cortex entrains epileptiform activity in CA1 in pilocarpine-treated rats. Neurobiol Dis. 2005;19:451-60.

105. Mello LE, Covolan L. Spontaneous seizures preferentially injure interneurons in the pilocarpine model of chronic spontaneous seizures. Epilepsy Res. 1996;26:123-9.

106. Scholl EA, Dudek FE, Ekstrand JJ. Neuronal degeneration is observed in multiple regions outside the hippocampus after lithium pilocarpine-induced status

epilepticus in the immature rat. Neuroscience. 2013;252:45-59.

107. Curia G, Longo D, Biagini G, Jones RS, Avoli M. The pilocarpine model of temporal lobe epilepsy. J Neurosci Methods. 2008;172:143-57.

108. Herzog AG. A relationship between particular reproductive endocrine disorders and the laterality of epileptiform discharges in women with epilepsy. Neurology. 1993;43:1907-10.

109. Holmes MD, Dodrill CB, Kutsy RL, Ojemann GA, Miller JW. Is the left cerebral hemisphere more prone to epileptogenesis than the right? Epileptic Disord. 2001;3:137-41.

110. Xia Y, Lai Y, Lei L, Liu Y, Yao D. Left hemisphere predominance of pilocarpine-induced rat epileptiform discharges. J Neuroeng Rehabil. 2009;6:42.

111. Vlooswijk MC, Vaessen MJ, Jansen JF, de Krom MC, Majoie HJ, Hofman PA, et al. Loss of network efficiency associated with cognitive decline in chronic epilepsy. Neurology. 2011;77:938-44.

112. Otte WM, Dijkhuizen RM, van Meer MP, van der Hel WS, Verlinde SA, van Nieuwenhuizen O, et al. Characterization of functional and structural integrity in experimental focal epilepsy: reduced network efficiency coincides with white matter changes. PLoS One. 2012;7:e39078.

113. Srinivas KV, Jain R, Saurav S, Sikdar SK. Small-world network topology of hippocampal neuronal network is lost, in an in vitro glutamate injury model of epilepsy. Eur J Neurosci. 2007;25:3276-86.

114. Brown JA, Terashima KH, Burggren AC, Ercoli LM, Miller KJ, Small GW, et al. Brain network local interconnectivity loss in aging APOE-4 allele carriers. Proc Natl Acad Sci U S A. 2011;108:20760-5.

115. Lo CY, Wang PN, Chou KH, Wang J, He Y, Lin CP. Diffusion tensor tractography reveals abnormal topological organization in structural cortical networks in Alzheimer's disease. J Neurosci. 2010;30:16876-85.

116. Zhao X, Liu Y, Wang X, Liu B, Xi Q, Guo Q, et al. Disrupted small-world brain networks in moderate Alzheimer's disease: a resting-state FMRI study. PLoS One. 2012;7:e33540.

117. Oyegbile TO, Dow C, Jones J, Bell B, Rutecki P, Sheth R, et al. The nature and course of neuropsychological morbidity in chronic temporal lobe epilepsy. Neurology. 2004;62:1736-42.

118. Helmstaedter C, Kurthen M, Lux S, Reuber M, Elger CE. Chronic epilepsy and cognition: a longitudinal study in temporal lobe epilepsy. Ann Neurol. 2003;54:425-32.

119. Kim YK, Lee DS, Lee SK, Kim SK, Chung CK, Chang KH, et al. Differential features of metabolic abnormalities between medial and lateral temporal lobe epilepsy: quantitative analysis of ^{18}F-FDG PET using SPM. J Nucl Med. 2003;44:1006-12.

120. Goffin K, Van Paesschen W, Dupont P, Van Laere K. Longitudinal microPET imaging of brain glucose metabolism in rat lithium-pilocarpine model of

epilepsy. Exp Neurol. 2009;217:205-9.

121. Lee EM, Park GY, Im KC, Kim ST, Woo CW, Chung JH, et al. Changes in glucose metabolism and metabolites during the epileptogenic process in the lithium-pilocarpine model of epilepsy. Epilepsia. 2012;53:860-9.

122. Jupp B, Williams J, Binns D, Hicks RJ, Cardamone L, Jones N, et al. Hypometabolism precedes limbic atrophy and spontaneous recurrent seizures in a rat model of TLE. Epilepsia. 2012;53:1233-44.

123. Choi JY, Kim SJ, Hong SB, Seo DW, Hong SC, Kim BT, et al. Extratemporal hypometabolism on FDG PET in temporal lobe epilepsy as a predictor of seizure outcome after temporal lobectomy. Eur J Nucl Med Mol Imaging. 2003;30:581-7.

124. Theodore WH, Sato S, Kufta CV, Gaillard WD, Kelley K. FDG-positron emission tomography and invasive EEG: seizure focus detection and surgical outcome. Epilepsia. 1997;38:81-6.

125. Nguyen DK, Nguyen DB, Malak R, Leroux JM, Carmant L, Saint-Hilaire JM, et al. Revisiting the role of the insula in refractory partial epilepsy. Epilepsia. 2009;50:510-20.

126. Isnard J, Guenot M, Ostrowsky K, Sindou M, Mauguiere F. The role of the insular cortex in temporal lobe epilepsy. Ann Neurol. 2000;48:614-23.

127. Dobesberger J, Ortler M, Unterberger I, Walser G, Falkenstetter T, Bodner T, et al. Successful surgical treatment of insular epilepsy with nocturnal

hypermotor seizures. Epilepsia. 2008;49:159-62.

128. Chen S, Fujita S, Koshikawa N, Kobayashi M. Pilocarpine-induced status epilepticus causes acute interneuron loss and hyper-excitatory propagation in rat insular cortex. Neuroscience. 2010;166:341-53.

129. Maccotta L, He BJ, Snyder AZ, Eisenman LN, Benzinger TL, Ances BM, et al. Impaired and facilitated functional networks in temporal lobe epilepsy. Neuroimage Clin. 2013;2:862-72.

130. Kettunen P, Krieger P, Hess D, El Manira A. Signaling mechanisms of metabotropic glutamate receptor 5 subtype and its endogenous role in a locomotor network. J Neurosci. 2002;22:1868-73.

131. Silverman JL, Smith DG, Rizzo SJ, Karras MN, Turner SM, Tolu SS, et al. Negative allosteric modulation of the mGluR5 receptor reduces repetitive behaviors and rescues social deficits in mouse models of autism. Sci Transl Med. 2012;4:131ra51.

132. Tuominen L, Nummenmaa L, Keltikangas-Jarvinen L, Raitakari O, Hietala J. Mapping neurotransmitter networks with PET: An example on serotonin and opioid systems. Hum Brain Mapp. 2013.

133. Kessler RM, Seibyl J, Cowan RL, Zald D, Young JS, Ansari MS, et al. Radiation Dosimetry of ^{18}F-FPEB in Humans. J Nucl Med. 2014.

134. Morimoto K, Fahnestock M, Racine RJ. Kindling and status epilepticus models of epilepsy: rewiring the brain. Prog Neurobiol. 2004;73:1-60.

135. Devinsky O, Vezzani A, Najjar S, De Lanerolle NC, Rogawski MA. Glia and epilepsy: excitability and inflammation. Trends Neurosci. 2013;36:174-84.

136. Pitkanen A, Kharatishvili I, Karhunen H, Lukasiuk K, Immonen R, Nairismagi J, et al. Epileptogenesis in experimental models. Epilepsia. 2007;48 Suppl 2:13-20.

137. Dickinson R, Peterson BK, Banks P, Simillis C, Martin JCS, Valenzuela CA, et al. Competitive inhibition at the glycine site of the N-methyl-D-aspartate receptor by the anesthetics xenon and isoflurane: evidence from molecular modeling and electrophysiology. Anesthesiology. 2007;107:756-67.

138. Yamakura T, Harris RA. Effects of gaseous anesthetics nitrous oxide and xenon on ligand-gated ion channels: Comparison with isoflurane and ethanol. Anesthesiology. 2000;93:1095-101.

139. Sou JH, Chan MH, Chen HH. Ketamine, but not propofol, anaesthesia is regulated by metabotropic glutamate 5 receptors. Br J Anaesth. 2006;96:597-601.

140. Volk H, Potschka H, Loscher W. Immunohistochemical localization of P-glycoprotein in rat brain and detection of its increased expression by seizures are sensitive to fixation and staining variables. J Histochem Cytochem. 2005;53:517-31.

141. Syvänen S, Labots M, Tagawa Y, Eriksson J, Windhorst AD, Lammertsma AA, et al. Altered GABAA Receptor Density and Unaltered Blood–Brain Barrier Transport in a Kainate Model of Epilepsy: An In Vivo Study Using ^{11}C-Flumazenil

and PET. J Nucl Med. 2012;53:1974-83.

142. Bankstahl JP, Bankstahl M, Kuntner C, Stanek J, Wanek T, Meier M, et al. A novel positron emission tomography imaging protocol identifies seizure-induced regional overactivity of P-glycoprotein at the blood–brain barrier. J Neurosci. 2011;31:8803-11.

요약 (국문초록)

필로카핀 유도 뇌전증 쥐 모델의 대사성글루타메이트 수용체5(mGluR5) 영상 및 뇌 대사 연결성 분석

최홍윤

서울대학교
융합과학기술대학원분자의학및바이오제약학과

목적

뇌전증은 다양한 신경전달물질 변화와 연관된 뇌네트워크 질환이다. 뇌전증에서흥분성 신경전달은 분자수준에서부터 뇌 전체의 연결을 포함하는 신경세포의 변화에 의해 생긴다. 그 가운데, 대사적글루타메이트 수용체 (Metabotropic glutamate receptor 5 −mGluR5) 는 뇌전증의글루타메이트 뇌신경 전달을 조절하는데 중요한 역할을 한다. 우리는 필로카핀 유도 측두엽 뇌전증 쥐 모델에서 mGluR5 이상 소견을 비침습적인 양전자단층촬영 (PET)

을 통해 획득하고자 하였다. 또한, 측두엽뇌전증은 뇌의 복잡한 네트워크와 연관이 되어 있다는 점으로부터 착안하여,뇌 대사 연결성 이상을 찾아내고자 하였다. 소동물 영상으로부터 새로운 다차원네트워크 해석 방법을 적용하였고, 향후 응용 가능성을 보고자 하였다. 종합적으로 본 연구에서는 mGluR5의 이상소견과 더불어 그 이상 영역들의 기능적 연결성을 통해 뇌전증의 네트워크 이상을 평가하는 방법을 제시하고자 한다. 또한, 본 연구에서는 분자 수준의 변화에서부터 뇌 전반의 네트워크 변화까지 통합하는 새로운 영상 분석 기법의 전임상적 응용 가능성을 보고자 한다.

방법

mGluR5 영상화를 위해 [^{11}C]ABP688 소동물용 PET/CT로 필로카핀 유도 뇌전증 쥐 모델과 대조군에서 영상을 획득하였다. 쥐 모델에서는 필로카핀 유도 뇌전증중첩증 이후 급성기, 아급성기 및 만성기에 영상을 획득하였다. mGluR5 수용체 결합능 (nondisplaceable binding potential, BP_{ND})을 단순화된 참조영역 구획모델을 활용하여 복셀기반의파라미터영상을 만들었다. 복셀기반의 통계적 비교분석을 통해 만성뇌전증쥐모델의 mGluR5 결합능 저하 영역을 찾아내었다. 또한, 뇌 대사 연결성 분석을 위해 [^{18}F]fluorodeoxyglucose PET을 만성뇌전증 쥐와 대조군에서 획득하였다. 이로부터국소뇌영역간의 대사적 상관성을 개체간 변화를 기반으로 계산하였

다. 그래프이론에 기반한 뇌 네트워크의 특성화 수치를 계산하고 비교하였다. 추가적으로, 새로운 네트워크 방법론으로서 다차원 위상수학 기반의 복잡뇌신경 해석 방법으로서 지속성상동 (persistent brain network homology)을 적용하여 문턱 값을 이용하지 않고 뇌 대사연결성을 비교하였다. 만성뇌전증쥐 모델군과대조군에서 single linkage distance(SLD)를 모든 네트워크 노드쌍에서 획득하고, 다차원 위상공간(metric space)에서 거리를 계산하였다. 한편, 글루타메이트 이상영역의 연결성을 조사하기 위하여 비침습적 PET을 통해 획득한 mGluR5의 이상영역 간의 대사적 상관성을 계산하고 두 그룹에서 비교하였다.

결과

[^{11}C]ABP688 PET을 이용해 mGluR5 결합능의뇌전증 발전 과정에 따른 변화를 측정하였다. 뇌전증중첩증 이후의 급성기에는 mGluR5결합능이 전체 뇌에서 저하되었다. 이후 아급성기에는피각과미상핵영역에서결합능이 회복되었으나 다른 영역은 여전히 저하되었다. 만성 뇌전증 시기에는 복셀기반평가시결합능이 일부 해마와 선조체에서 저하되었다. 만성 뇌전증모델군과 대조군 사이의 FDG PET을 활용한 뇌 대사 연결성을 평가하였을 때, 뇌전증 군에서는 영역별 상관성이 좌측 선조체와내후각피질을 포함한 곳이 유의하게 저하되었다. 그래프이론 기반 파라미터들인노드-효율성 및 지역-효율성을 비교

시뇌전증모델에서 유의하게 좌측 선조체에서 저하되어있었다. 지속성 상동기반의 모델링을 통한 위상공간에서 거리를 비교시뇌전증모델군에서 좌측 섬엽/선조체와 양측 대뇌피질/심부피질 연결들이 멀어지는 경향을 보였다. 한편, mGluR5 결합능이 유의하게 저하된 영역들 사이의 연결성을 평가하였을 때, 각 영역은 대조군에서는 매우 높은 상관성을 보였으나, 뇌전증모델군에서는 그 연결성의 저하가 관찰되었다.

결론

비침습적 mGluR5영상을 통해 양측 해마 및 선조체에서 mGluR5결합능 이상 소견이 뇌전증 모델에서 관찰되었다. 쥐의 뇌전증 모델에서는 전반적으로 뇌의 연결성이 저하된 것이 관찰되었으며, 특히 좌측 변연계-주위변연계-대뇌피질로 이어지는 네트워크의 이상이 관찰되었다. 이러한 mGluR5의 변화와 뇌 대사 연결성 변화를 찾아낸 본 연구는 다기능적 영상기법을 통해 전임상단계에서복잡뇌 네트워크를 해석할 수 있을 가능성을 제시할 수 있다.

Keywords: 뇌전증, mGluR5, [^{11}C]ABP688, 뇌대사연결성, 그래프이론, Persistent Homology

Student number: 2011-23073